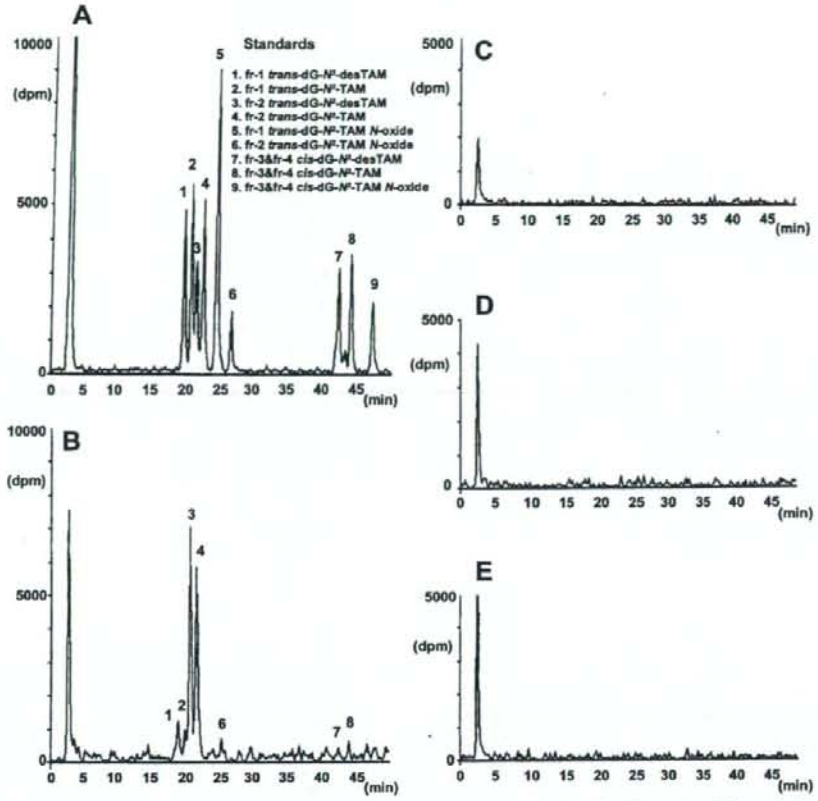

Figure 4. ^{32}P-Postlabeling/HPLC analysis for determination of DNA adducts in rat liver. The hepatic DNA was used for analysis of DNA adducts using ^{32}P-postlabeling/HPLC, as described in the Materials and Methods. Standards (A), TAM (B), control (C), TOR (D), and RAL (E).

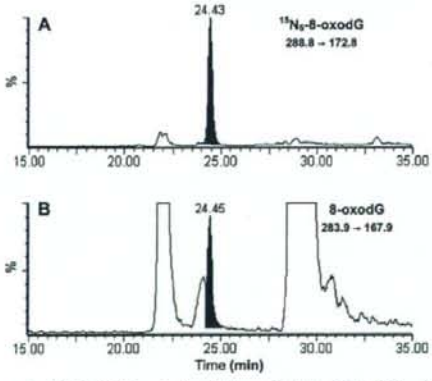

Figure 5. LC/MS/MS analysis of 8-oxodG. The DNA (50 μg) was mixed with $^{15}N_5$-8-oxodG (500 pg) and digested with nuclease P1 and alkaline phosphatase in a buffer. The resulting nucleosides were analyzed using LC/MS/MS, as described in the Materials and Methods. Quantative analysis of $^{15}N_5$-8-oxodG and 8-oxodG was achieved by monitoring the MS/MS transitions corresponding to the loss of deoxyribose from $^{15}N_5$-8-oxodG (*m/z* 288.8 → 172.8) (A) and 8-oxodG (*m/z* 283.8 → 167.8) (B), respectively. The amount of 8-oxodG in DNA samples was determined by comparing with $^{15}N_5$-8-oxodG.

Table 1. Level of Hepatic 8-OxodG Adducts in Rats Treated with Antiestrogens[a]

	8-oxodG (adducts/10^6 dNs)
control	1.78 ± 0.51 (100%)
TAM	2.17 ± 0.36 (122%)
4-OHTAM	1.97 ± 0.14 (111%)
TOR	1.82 ± 0.33 (102%)
RAL	1.92 ± 0.35 (108%)
ICI 182,780	1.80 ± 0.39 (101%)

[a] Data are expressed as mean values ± SD from three rats.

did not promote bulky DNA adducts in the liver. Our results are consistent with the fact that TOR promoted 2 orders of magnitude lower levels of DNA adducts in rat liver as compared to TAM (*14*, *31*). We found previously that TOR is α-hydoxylated 6-fold higher by cytochrome 3A4 than TAM (*42*), but unlike α-hydroxytamoxifen (α-OHTAM), α-OHTOR is not a substrate for hydroxysteroid sulfotransferase and the reactivity of α-acetoxyTOR, a model activated from TOR, with DNA was much less than that of α-acetoxyTAM (*43*). In addition, like TAM, TOR did not promote oxidative DNA damage. Therefore, TOR may not have genotoxic potential. In fact, no mutagenic events were detected in liver of λ/lacI rats treated with TOR (*44*). Only one out of 21 patients treated with TOR had a K-*ras* mutation whereas a high frequency of K-*ras* mutation was detected in endometrial tissues of patients treated with TAM (*23*). The replacement of TAM by TOR may minimize the development of endometrial cancer observed in women treated with TAM.

In this study, we could not detect significant bulky and oxidative DNA adducts induced by RAL or ICI 182,780 in the rat livers. Actually, no increased incidence of endometrial cancer was observed in women treated with RAL (*45*, *46*). Because RAL and ICI 182,780 have only a minimal estrogenic activity (*47*, *48*), use of both compounds may have a more clinical benefit for breast cancer therapy and prevention. However, because RAL has two hydroxyl moieties in the structure, the hydroxylated compound can rapidly conjugate through phase II metabolism and get excreted. As a result, higher doses may be required to be administered in humans to obtain an efficacy equivalent to that with TAM (*49*). ICI 182,780 is highly lipophilic and does not ionize at physical conditions (*50*). This may make it difficult for humans to reach adequate bioavailability by oral administration.

Only TAM generated a significant amount of DNA adducts. If the mutagenic TAM−DNA adducts are not efficiently repaired, TAM−DNA adducts could accumulate for extended periods in the targeted tissues, leading to the development of cancers (*51*). TOR, RAL, and ICI 182,780 were observed to be less genotoxic than TAM. Although the effects of these antiestrogens on ER pathways should be evaluated, TOR, RAL, and ICI 182,780 may be safer alternatives for breast cancer therapy and chemoprevention.

Acknowledgment. This study was supported in part by the National Institute of Environmental Health Sciences Grants ES09418 and ES012408.

References

(1) Lewis, J. S., and Jordan, V. C. (2005) Selective estrogen receptor modulators (SERMs): Mechanisms of anticarcinogenesis and drug resistance. *Mutat. Res. 591*, 247−263.

(2) Killackey, M., Hakes, T. B., and Pierce, V. K. (1985) Endometrial adenocarcinoma in breast cancer patients receiving antiestrogens. *Cancer Treat. Rep. 69*, 237−238.

(3) van Leeuwen, F. E., Benraadt, J., Coebergh, J. W. W., Kiemeney, L. A. L. M., Diepenhorst, F. W., van den Belt-Dusebout, A. W., and van Tinteren, H. (1994) Risk of endometrial cancer after tamoxifen treatment of breast cancer. *Lancet 343*, 448−452.

(4) Fischer, B., Costantino, J. P., Wickerham, L., Redmond, C. K., Kavanah, M., Cronin, W. M., Botel, V., Robidoux, A., Dimitrov, N., Atkins, J., Daly, M., Wieand, S., Tan-Chiu, E., Ford, L., Wormark, N., and et al. (1998) Tamoxifen for prevention of breast cancer: report of the National Surgical Adjuvant Breast and Bowel Project P-1 Study. *J. Natl. Cancer Inst. 90*, 1371−1388.

(5) Bernstein, L., Deapen, D., Cerhan, J. R., Schwartz, S. M., Liff, J., McGann-Maloney, E., Perlman, J. A., and Ford, L. (1999) Tamoxifen therapy for breast cancer and endometrial cancer risk. *J. Natl. Cancer Inst. 91*, 1654−1662.

(6) Stygar, D., Muravitskaya, N., Eriksson, B., Eriksson, H., and Sahlin, L. (2003) Effects of SERM (selective estrogen receptor modulator) treatment on growth and proliferation in the rat uterus. *Reprod. Biol. Endcrinol. 1*, 1−8.

(7) Harvey, H. A., Kimura, M., and Hajba, A. (2006) Toremifene: An evaluation of its safety profile. *Breast* Nov 8, Epub ahead of print.

(8) Kim, S. Y., Suzuki, N., Laxmi, Y. R. S., and Shibutani, S. (2004) Genotoxic mechanism of tamoxifen in developing endometrial cancer. *Drug Metab. Rev. 36*, 199−218.

(9) Han, X., and Liehr, J. G. (1992) Induction of covalent DNA adducts in rodents by tamoxifen. *Cancer Res. 52*, 1360−1363.

(10) Osborne, M. R., Hewer, A., Hardcastle, I. R., Carmichael, P. L., and Phillips, D. H. (1996) Identification of the major tamoxifen-deoxyguanosine adduct formed in the liver DNA of rats treated with tamoxifen. *Cancer Res. 56*, 66−71.

(11) Divi, R. L., Osborne, M. R., Hewer, A., Phillips, D. H., and Poirier, M. C. (1999) Tamoxifen-DNA adduct formation in rat liver determined by immunoassay and ^{32}P-postlabeling. *Cancer Res. 59*, 4829−4833.

(12) Umemoto, A., Komaki, K., Monden, Y., Suwa, M., Kanno, Y., Kitagawa, M., Suzuki, M., Lin, C.-X., Ueyama, Y., Momen, M. A., Ravindernath, A., and Shibutani, S. (2001) Identification and quantification of tamoxifen-DNA adducts in the liver of rats and mice. *Chem. Res. Toxicol. 14*, 1006−1013.

(13) Greaves, P., Goonetilleke, R., Nunn, G., Topham, J., and Orton, T. (1993) Two-year carcinogenicity study of tamoxifen in Alderley Park Wister-derived rats. *Cancer Res. 53*, 3919−3924.

(14) Hard, G. C., Iatropoulos, M. J., Jordan, K., Radi, L., Kaltenberg, O. P., Imondi, A. R., and Williams, G. M. (1993) Major difference in the hepatocarcinogenicity and DNA adduct forming ability between toremifene and tamoxifen in female Crl:CD(BR) rats. *Cancer Res. 53*, 4534−4541.

(15) Rajaniemi, H., Rasanen, I., Koivisto, P., Peltonen, K., and Hemminki, K. (1999) Identification of the major tamoxifen-DNA adducts in rats liver by mass spectroscopy. *Carcinogenesis 20*, 305−309.

(16) Poirier, M. C., and Schild, L. J. (2003) The toxicity of tamoxifen: Extent and consequences, Kona, Hawaii, January 23, 2003. *Mutagenesis 18*, 395−399.

(17) Marnett, L. J. (2005) Letter to the Editor. *Chem. Res. Toxicol. 18*, 1507−1511.

(18) Shibutani, S., Ravindernath, A., Suzuki, N., Terashima, I., Sugarman, S. M., Grollman, A. P., and Pearl, M. L. (2000) Identification of tamoxifen-DNA adducts in the endometrium of women treated with tamoxifen. *Carcinogenesis 21*, 1461−1467.

(19) Martin, E. A., Brown, K., Gaskell, M., Al-Azzawi, F., Garner, R. C., Boocock, D. J., Mattock, E., Pring, D. W., Dingley, K., Turteltaub, K. W., Smith, L. L., and White, I. N. (2003) Tamoxifen DNA damage detected in human endometrium using accelerator mass spectrometry. *Cancer Res. 63*, 8461−8465.

(20) Carmichael, P. L., Ugwumadu, A. H., Neven, P., Hewer, A. J., Poon, G. K., and Phillips, D. H. (1996) Lack of genotoxicity of tamoxifen in human endometrium. *Cancer Res. 56*, 1475−1479.

(21) Carmichael, P. L., Sardar, S., Crooks, N., Neven, P., Van Hoof, I., Ugwumadu, A., Bourne, T., Tomas, E., Hellberg, P., Hewer, A. J., and Phillips, D. H. (1999) Lack of evidence from HPLC ^{32}P-postlabeling for tamoxifen-DNA adducts in the human endometrium. *Carcinogenesis 20*, 339−342.

(22) Beland, F. A., Churchwell, M. I., Doerge, D. R., Parkin, D. R., Malejka-Giganti, D., Hewer, A., Phillips, D. H., Carmichael, P. L., Gamboa da Costa, G., and Marques, M. M. (2004) Electrospray ionization-tandem mass spectrometry and ^{32}P-postlabeling analyses of tamoxifen-DNA adducts in humans. *J. Natl. Cancer Inst. 96*, 1099−1104.

(23) Hachisuga, T., Tsujioka, H., Horiuchi, S., Udou, T., Emoto, M., and Kawarabayashi, T. (2005) K-*ras* mutation in the endometrium of tamoxifen-treated breast cancer patients, with a comparison of tamoxifen and toremifene. *Br. J. Cancer 92*, 1098−1103.

(24) Terashima, I., Suzuki, N., and Shibutani, S. (1999) Mutagenic potential of α-(*N*^{2}-deoxyguanosinyl)tamoxifen lesions: The major DNA adducts detected in endometrial tissues of patients treated with tamoxifen. *Cancer Res. 59*, 2091−2095.

(25) Marques, M. M., and Beland, F. A. (1997) Identification of tamoxifen-DNA adducts formed by 4-hydroxytamoxifen quinone methide. *Carcinogenesis 18*, 1949−1954.

(26) Dehal, S. S., and Kupfer, D. (1999) Cytochrome P-450 3A and 2D6 catalyze ortho hydroxylation of 4-hydroxytamoxifen and 3-hydroxytamoxifen (droloxifene) yielding tamoxifen catechol: Involvement of catechols in covalent binding to hepatic proteins. *Drug Metab. Dispos. 27*, 681−688.

(27) Zhang, F., Fan, P. W., Liu, X., Shen, L., van Breemen, R. B., and Bolton, J. L. (2000) Synthesis and reactivity of a potential carcinogenic metabolite of tamoxifen: 3,4-Dihydroxytamoxifen-*o*-quinone. *Chem. Res. Toxicol. 13*, 53−62.

(28) Ye, Q., and Bodell, W. J. (1996) Production of 8-hydroxy-2′-deoxguanosine in DNA by microsomal activation of tamoxifen and 4-hydroxytamoxifen. *Carcinogenesis 17*, 1747−1750.

(29) Okubo, T., Nagai, F., Ushiyama, K., Yokoyama, Y., Ozawa, S., Kano, K., Tomita, S., Kubo, H., and Kano, I. (1998) DNA cleavage and 8-hydroxydeoxyguanosine formation caused by tamoxifen derivatives in vitro. *Cancer Lett. 122*, 9−15.

(30) Buzdar, A. U., and Hortobagyi, G. N. (1998) Tamoxifen and toremifene in breast cancer: Comparison of safety and efficacy. *J. Clin. Oncol. 16*, 348−353.

(31) White, I. N., de Matteis, F., Davies, A., Smith, L. L., Crofton-Sleigh, C., Venitt, S., Hewer, A., and Phillips, D. H. (1992) Genotoxic potential of tamoxifen and analogues in female Fischer F344/n rats, DBA/2 and C57BL/6 mice and in human MCL-5 cells. *Carcinogenesis 13*, 2197−2203.

(32) Vogel, V. G., Costantino, J. P., Wickerham, D. L., Cronin, W. M., and Wolmark, N. (2002) The study of tamoxifen and raloxifene: Preliminary enrollment data from a randomized breast cancer risk reduction trial. *Clin. Breast Cancer 3*, 153−159.

(33) Yu, L., Liu, H., Li, W., Zhang, F., Luckie, C., van Breemen, R. B., Thatcher, G. R. J., and Bolton, J. L. (2004) Oxidation of raloxifene to quinoids: Potential toxic pathways via a diquinone methide and *o*-quinones. *Chem. Res. Toxicol. 17*, 879−888.

(34) Bowler, J., Lilley, T. J., Pittam, J. D., and Wakeling, A. E. (1989) Novel steroidal pure antiestrogens. *Steroids 54*, 71−99.
(35) Howell, A., DeFriend, D., Robertson, J., Blamey, R., and Walton, P. (1995) Response to a specific antioestrogen (ICI 182,780) in tamoxifen-resistant breast cancer. *Lancet 345*, 29−30.
(36) Shibutani, S., Dasaradhi, L., Terashima, I., Banoglu, E., and Duffel, M. W. (1998) α-Hydroxytamoxifen is a substrate of hydroxysteroid (alcohol) sulfotransferase, resulting in tamoxifen DNA adducts. *Cancer Res. 58*, 647−653.
(37) Terashima, I., Suzuki, N., and Shibutani, S. (2002) ^{32}P−Postlabeling/polyacrylamide gel electrophoresis analysis: Application to the detection of DNA adducts. *Chem. Res. Toxicol. 15*, 305−311.
(38) Wang, L., Hirayasu, K., Ishizawa, M., and Kobayashi, Y. (1994) Purification of genomic DNA from human whole blood by 2-propanol-fractionation with concentrated NaI and SDS. *Nucleic Acids Res. 22*, 1774−1775.
(39) Schuler, D., Otteneder, M., Sagelsdorff, P., Eder, E., Gupta, R. C., and Lutz, W. K. (1997) Comparative analysis of 8-oxo-2′-deoxyguanosine in DNA by ^{32}P-postlabeling and electrochemical detection. *Carcinogenesis 18*, 2367−2371.
(40) Beland, F. A., McDaniel, L. P., and Marques, M. M. (1999) Comparison of the DNA adducts formed by tamoxifen and 4-hydroxytamoxifen in vivo. *Carcinogenesis 20*, 471−477.
(41) Churchwell, M. I., Beland, F. A., and Doerge, D. R. (2002) Quantification of multiple DNA adducts formed through oxidative stress using liquid chromatography and electrospray tandem mass spectrometry. *Chem. Res. Toxicol. 15*, 1295−1301.
(42) Kim, S. Y., Suzuki, N., Laxmi, Y. R. S., Rieger, R., and Shibutani, S. (2003) α-Hydroxylation of tamoxifen and toremifene by human and rat cytochrome P450 3A subfamily enzymes. *Chem. Res. Toxicol. 16*, 1138−1144.
(43) Shibutani, S., Ravindernath, A., Terashima, I., Suzuki, N., Laxmi, Y. R. S., Kanno, Y., Suzuki, M., Apak, T. I., Sheng, J. J., and Duffel, M. W. (2001) Mechanism of lower genotoxicity of toremifene compared with tamoxifen. *Cancer Res. 61*, 3925−3931.
(44) Davies, R., Oreffo, V. I. C., Martin, E. A., Festing, M. F. W., White, I. N. H., Smith, L. L., and Styles, J. A. (1997) Tamoxifen causes gene mutations in the livers of *λ/lacI* transgenic rats. *Cancer Res. 57*, 1288−1293.
(45) Cummings, S. R., Eckert, S., Krueger, K. A., Grady, D., Powles, T. J., Cauley, J. A., Norton, L., Nickelsen, T., Bjarnason, N. H., Morrow, M., Lippman, M. E., Black, D., Glusman, J. E., Costa, A., and Jordan, V. C. (1999) The effect of raloxifene on risk of breast cancer in postmenopausal women: Results from the MORE randomized trial. Multiple Outcomes of Raloxifene Evaluation. *JAMA 281*, 2189−2197.
(46) Cauley, J. A., Norton, L., Lippman, M. E., Eckert, S., Krueger, K. A., Purdie, D. W., Farrerons, J., Karasik, A., Mellstrom, D., Ng, K. W., Stepan, J. J., Powles, T. J., Morrow, M., Costa, A., Silfen, S. L., Walls, E. L., Schmitt, H., Muchmore, D. B., Jordan, V. C., and Ste-Marie, L. G. (2001) Continued breast cancer risk reduction in postmenopausal women treated with raloxifene: 4-Year results from the MORE trial. Multiple outcomes of raloxifene evaluation. *Breast Cancer Res. Treat. 65*, 125−134.
(47) Delmas, P. D., Bjarnason, N. H., Mitlak, B. H., Ravoux, A. C., Shah, A. S., Huster, W. J., Draper, M., and Christiansen, C. (1997) Effects of raloxifene on bone mineral density, serum cholesterol concentrations, and uterine endometrium in postmenopausal women. *N. Engl. J. Med. 337*, 1641−1647.
(48) Bross, P. F., Baird, A., Chen, G., Jee, J. M., Lostritto, R. T., Morse, D. E., Rosario, L. A., Williams, G. M., Yang, P., Rahman, A., Williams, G., and Pazdur, R. (2003) Fulvestrant in postmenopausal women with advanced breast cancer. *Clin. Cancer Res. 9*, 4309−4317.
(49) Gottardis, M. M., and Jordan, V. C. (1987) Antitumor actions of keoxifene and tamoxifen in the *N*-nitrosomethylurea-induced rat mammary carcinoma model. *Cancer Res. 47*, 4020−4024.
(50) Howell, A., Osborne, C. K., Morris, C., and Wakeling, A. E. (2000) ICI 182,780 (Faslodex): Development of a novel, "pure" antiestrogen. *Cancer 89*, 817−825.
(51) Kim, S. Y., Suzuki, N., Laxmi, Y. R. S., and Shibutani, S. (2006) Inefficient repair of tamoxifen-DNA adducts in rats and mice. *Drug Metab. Dispos. 34*, 311−317.

TX060052N

In vivo mutagenicity and initiation following oxidative DNA lesion in the kidneys of rats given potassium bromate

Takashi Umemura,[1,4] Keita Kanki,[1] Yuichi Kuroiwa,[1] Yuji Ishii,[3] Keita Okano,[3] Takehiko Nohmi,[2] Akiyoshi Nishikawa[1] and Masao Hirose[1]

Divisions of [1]Pathology and [2]Genetics and Mutagenesis, National Institute of Health Sciences, 1-18-1 Kamiyoga, Setagaya-ku, Tokyo 158-8501; and [3]Faculty of Pharmaceutical Science, Department of Analytical Chemistry, Hoshi University, 2-4-41 Ebara, Shinagawa-ku, Tokyo 142-8501, Japan

(Received February 17, 2006/Revised April 21, 2006/Accepted May 1, 2006/Online publication June 29, 2006)

To clarify the role of 8-OHdG formation as a starting point for carcinogenesis, we examined the dose-dependence and time-course of changes of *OGG1* mRNA expression, 8-OHdG levels and *in vivo* mutations in the kidneys of *gpt* delta rats given $KBrO_3$ in their drinking water for 13 weeks. There were no remarkable changes in *OGG1* mRNA in spite of some increments being statistically significant. Increases of 8-OHdG occurred after 1 week at 500 p.p.m. and after 13 weeks at 250 p.p.m. Elevation of Spi$^-$ mutant frequency, suggestive of deletion mutations, occurred after 9 weeks at 500 p.p.m. In a two-stage experiment, F344 rats were given $KBrO_3$ for 13 weeks then, after a 2-week recovery, treated with 1% NTA in the diet for 39 weeks. The incidence and multiplicity of renal preneoplastic lesions in rats given $KBrO_3$ at 500 p.p.m. followed by NTA treatment were significantly higher than in rats treated with NTA alone. Results suggest that a certain period of time might be required for 8-OHdG to cause permanent mutations. The two-step experiment shows that cells exposed to the alteration of the intranuclear status by oxidative stress including 8-OHdG formation might be able to form tumors with appropriate promotion. (*Cancer Sci* 2006; 97: 829–835)

Oxidative DNA damage is caused by reactive oxygen species derived from various processes of cellular metabolism, especially metabolism of exogenous mutagens and carcinogens. 8-OHdG, a form of guanine oxidized at the C-8 position, is believed to be fairly stable and the most abundant oxidative lesion[1] among the many oxidized nucleosides known. It is established that 8-OHdG lesions are repaired mainly by the so-called GO system.[2] In this system: OGG1 DNA glycosylase and apurinic/apyrimidic lyase act to correct 8-OH-G:C pairs;[3] MYH glycosylase removes an A base mispaired with 8-OHdG;[4] and MTH 8-OH-dGTpase hydrolyzes 8-OH-dGTP in the nucleotide pool for prevention of its incorporation into DNA.[5] Thus, the existence of these three genes for repair of 8-OHdG in DNA points to 8-OHdG as a biologically deleterious base lesion. Induction of *OGG1* mRNA expression and an increase of OGG1 activity following application of exogenous oxidative stimuli have been demonstrated.[6–9]

$KBrO_3$, which induces renal cell tumors in F344 rats after oral administration at concentrations of 250 and 500 p.p.m,[10] has been classified as a genotoxic carcinogen based on positive mutagenicity in the Ames,[11] chromosome aberration,[12] and micronucleus[13] tests. Effective prevention of $KBrO_3$ clastogenicity by antioxidants,[14,15] and induction of 8-OHdG by $KBrO_3$ *in vitro* and *in vivo* strongly suggest that 8-OHdG plays a key role in $KBrO_3$ mutagenesis and carcinogenesis.[16–19] $KBrO_3$ has therefore received much attention as a suitable agent for research into 8-OHdG-related carcinogenesis. With a single dose of $KBrO_3$ by i.p. injection, 8-OHdG glycosylase activity in the rat kidney is increased in association with 8-OHdG formation.[20] A recent study using *OGG1*-deficient *gpt* delta mice found high amounts of 8-OHdG in the genome DNA and GC:TA transversion mutations following $KBrO_3$ exposure at a concentration of 2000 p.p.m. for 12 weeks.[21] However, a single high dose of $KBrO_3$ (300 mg/kg) did not induce tumors in rats,[22] and its carcinogenicity in mice is equivocal.[23] Therefore, interpretation of data for 8-OHdG and consequent mutations with reference to their significance for carcinogenesis is difficult.

Our aim is to determine conditions required for cells with 8-OHdG that survive specific repair systems to develop mutations and have tumor-initiating potential. For this purpose, carcinogenic doses of $KBrO_3$ were administered in drinking water and the dose-dependence and time-course of changes in *OGG1* mRNA expression, 8-OHdG levels and *in vivo* MFs in the kidneys of *gpt* delta rats were measured. In a second experiment, F344 rats were given NTA as a kidney tumor-promoter,[24] in a two-stage rat renal carcinogenesis experiment to assess tumor-initiation activity of $KBrO_3$ given at the same doses as in the first experiment.

Materials and methods

Chemicals

$KBrO_3$ and NTA were purchased from Wako Pure Chemical Industries (Osaka, Japan) and Tokyo Kasei (Tokyo, Japan),

[4]To whom correspondence should be addressed. E-mail: umemura@nihs.go.jp

Abbreviations: 6-TG, 6-thioguanine; 8-OHdG, 8-hydroxydeoxyguanosine; AHs, atypical hyperplasias; ATs, atypical tubules; BD, basal diet; H–E, hematoxylin–eosin; $KBrO_3$, potassium bromate; dG, deoxyguanosine; DW, distilled water; MFs, mutant frequencies; NTA, nitrilotriacetic acid trisodium salt; PCR, polymerase chain reaction; p.p.m., parts per million; RCTs, renal cell tumors; SD, standard deviation.

doi: 10.1111/j.1349-7006.2006.00248.x

respectively. Alkaline phosphatase was obtained from Sigma Chemical (St. Louis, MO, USA) and nuclease P1 was from Yamasa Shoyu (Chiba, Japan).

Animals, diet and housing conditions

The protocol for this study was approved by the Animal Care and Utilization Committee of the National Institute of Health Sciences (Tokyo, Japan). Five-week-old male *gpt* delta rats carrying approximately 10 tandem copies of the transgene lambda EG10 per haploid genome and F344 rats were obtained from Japan SLC (Shizuoka, Japan) and from Charles River Japan (Kanagawa, Japan), respectively. They were housed in polycarbonate cages (five rats per cage) with hardwood chips for bedding in a conventional animal facility, maintained under conditions of controlled temperature (23 ± 2°C), humidity (55 ± 5%), air change (12 times per hour), and lighting (12 h light/dark cycle) and were given free access to CRF-1 BD (Charles River Japan) and tap water.

Animal treatment

Experiment I. Groups of five male gpt delta rats were given $KBrO_3$ solution at concentrations of 0, 60, 125, 250 and 500 p.p.m. in the drinking water for 13 weeks. Additional subgroups of five male *gpt* delta rats were given $KBrO_3$ solution at a dose of 500 p.p.m. in the drinking water for 1, 5 or 9 weeks. At the end of each period, the animals were killed under ethyl ether anesthesia and a part of one kidney was homogenized in Isogen (Nippon Gene, Tokyo, Japan) and stored at −80°C until used for isolation of total RNA. The remaining kidney was also stored at −80°C for 8-OHdG measurement and *in vivo* mutation assays.

Experiment II. F344 rats were used in the tumor initiation study rather than Sprague–Dawley rats, a back strain of *gpt* delta rats, because of the accumulated data on the effects of $KBrO_3$ on the former strain. Ninety F344 male rats were randomly divided into seven groups. Fifteen animals each in groups 2–5 were given $KBrO_3$ at concentrations of 60, 125, 250 and 500 p.p.m. for 13 weeks. After a 2-week recovery period, rats received NTA as a promoter at a concentration of 1% in the diet for 37 weeks. Ten animals each in groups 1 and 6 were given DW in place of $KBrO_3$, followed by the NTA regimen at doses of 0 and 1%, respectively. Additionally, 10 animals in group 7 were maintained untreated following $KBrO_3$ treatment at a concentration of 500 p.p.m. for 13 weeks until the end of the experiment. Rats were killed at week 52 under ethyl ether anesthesia and the kidneys were removed immediately and fixed in 10% buffered formalin.

Real-time reverse transcription–PCR for mRNA of *OGG1*

Total mRNA was isolated using the Isogen total mRNA isolation reagent (Nippon Gene) according to the manufacturer's instructions. After reverse-transcription with random hexamers using an SYBR RT-PCR Kit (Takara Bio, Shiga, Japan), PCR was carried out with specific primers for rat *OGG1* (5′-CAACATTGCTCGCATCACTGG-3′ and 5′-ATGGCTTTAGCACTGGCACATACA-3′) (Smart Cycler; Cepheid, Sunnyvale, CA) and r*GAPDH* (5′-GACAACTTTG-GCATCGTGGA-3′ and 5′-ATGCAGGGATGATGTTCTGG-3′) (Ex Taq, RT-PCR version; Takara Bio). Real-time monitoring of PCR products was achieved with fluorescence of SYBR green I (Takara Bio), and expression levels of *OGG1* were determined as ratios to *GAPDH* levels obtained with the same master reaction.[25] All of the procedures after isolation of total RNA were carried out at the Dragon Genomics Center of Takara Bio (Mie, Japan).

Measurement of nuclear 8-OHdG

In order to prevent 8-OHdG formation as a by-product during DNA isolation,[26] kidney DNA was extracted using a slight modification of the method of Nakae *et al.*[27] Briefly, nuclear DNA was extracted with a commercially available DNA Extracter WB Kit (Wako Pure Chemical Industries) containing an antioxidant NaI solution to dissolve cellular components. For further prevention of auto-oxidation in the cell lysis step, deferoxamine mesylate (Sigma Chemical) was added to the lysis buffer.[28] The DNA was digested to deoxynucleotides with nuclease P1 and alkaline phosphatase and levels of 8-OHdG (8-OHdG/10^5 dG) were measured by high-performance liquid chromatography with an electrochemical detection system (Coulochem II; ESA, Bedford, MA).

In vivo mutation assays

6-TG and Spi$^-$ (insensitive P2 interference) selection was carried out as previously described.[29] Briefly, genomic DNA was extracted from the kidneys, and lambda EG10 DNA (48 kb) was rescued as the lambda phage by *in vitro* packaging. For 6-TG selection, the packaged phage was incubated with *Escherichia coli* YG6020, expressing Cre recombinase, and converted to a plasmid carrying *gpt* and chloramphenicol acetyltransferase. Infected cells were mixed with molten soft agar and poured onto agar plates containing chloramphenicol and 6-TG. In order to determine the total number of rescued plasmids, infected cells were also poured on plates containing chloramphenicol without 6-TG. The plates were incubated at 37°C for the selection of 6-TG-resistant colonies, and the *gpt* MF was calculated by dividing the number of *gpt* mutants after clonal correction by the number of rescued phages.

For Spi$^-$ selection, the packaged phage was incubated with *E.coli* XL-1 Blue MRA for survival titration and *E.coli* XL-1 Blue MRA P2 for mutant selection. Infected cells were mixed with molten lambda-trypticase soft agar and poured onto lambda-trypticase agar plates. The plaques (Spi$^-$ candidates) detected on the plates were suspended in SM buffer. In order to confirm the Spi$^-$ phenotype of candidates, the suspensions were spotted on three types of plates containing XL-1 Blue MRA, XL-1 Blue MRA P2, or WL95 P2 strains and were spread with soft agar. The numbers of mutants that made clear plaques on each plate were counted as confirmed Spi$^-$ mutants. The Spi$^-$ MF was calculated by dividing the number of Spi$^-$ mutants by the number of rescued phages.

Histopathology for the initiation bioassay

Formalin-fixed kidneys were processed for embedding in paraffin and sectioned at 2 μm. Sections were routinely stained with H–E for histopathological assessment. All sections were coded and read without knowledge of the treatment for counting of ATs, AHs and RCTs. The

doi: 10.1111/j.1349-7006.2006.00248.x

diagnostic criteria for preneoplastic and neoplastic lesions of the kidney proposed by Dietrich and Swenberg,[30] were used to distinguish ATs, AHs and RCTs.

Statistics

The significance of differences in the results for mRNA levels of *OGG1*, 8-OH-dG levels and MFs was evaluated with ANOVA, followed by Dunnett's multiple comparison test. The significance of differences in the multiplicity of lesions in the initiation bioassay was evaluated using Tukey's test, and that for incidences with Fisher's exact probability test.

Results

Experiment I

OGG1 *mRNA expression.* Figure 1(a) illustrates changes of *OGG1* mRNA expression in kidneys of *gpt* delta rats given $KBrO_3$ solution at concentrations of 0, 60, 125, 250 and 500 p.p.m. in the drinking water for 13 weeks. Significant ($P < 0.05$) elevation of expression occurred at 250 p.p.m. At 500 p.p.m., a significant increase of expression ($P < 0.01$) was evident 5 weeks after the start of the exposure (Fig. 1b).

8-OHdG levels. Figure 2(a) shows data for 8-OHdG levels in kidneys of *gpt* delta rats given $KBrO_3$ in the drinking water for 13 weeks. 8-OHdG levels were elevated compared to the control value (0.28 ± 0.06 8-OHdG/10^5 dG) at $KBrO_3$ concentrations of 250 and 500 p.p.m. in a clearly dose-dependent manner (250 p.p.m., 0.45 ± 0.19 8-OHdG/10^5 dG, $P < 0.05$; 500 p.p.m., 0.59 ± 0.16 8-OHdG/10^5 dG, $P < 0.01$). Figure 2(b) summarizes the data from kidneys of *gpt* delta rats given $KBrO_3$ solution at a concentration of 500 p.p.m. for 1, 5, 9 and 13 weeks. 8-OHdG levels increased with time, with a peak at week 5 and a gradual decrease thereafter. All of the 8-OHdG levels for the treated rats were statistically significant ($P < 0.01$) compared to the control value (1 week, 0.54 ± 0.10 8-OHdG/10^5 dG; 5 weeks, 0.88 ± 0.10 8-OHdG/10^5 dG; 9 weeks, 0.75 ± 0.02 8-OHdG/10^5 dG).

In vivo *mutations.* Changes in *gpt* and Spi$^-$ MFs in *gpt* delta rats given $KBrO_3$ solution for 13 weeks are shown in Figs 3 and 4. There was no statistically significant increment in *gpt* MFs among the treated animals in spite of the dose-dependent increase of 8-OHdG observed in rats treated with 250 p.p.m. $KBrO_3$ (Fig. 3a,b). In contrast, Spi$^-$ MF in rats

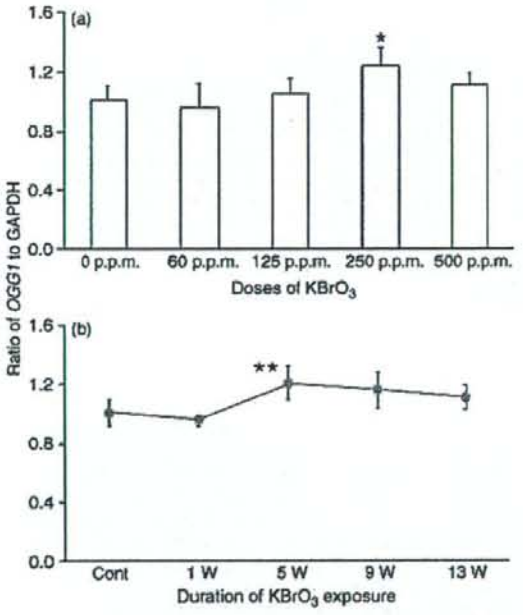

Fig. 1. (a) Dose-dependent expression of *OGG1* mRNA in kidneys of *gpt* delta rats given $KBrO_3$ at concentrations of 0, 60, 125, 250 and 500 p.p.m. in their drinking water for 13 weeks. Values are means ± SD of data for five rats. $^*P < 0.05$, significantly different from the controls (0 p.p.m.). (b) Time-course of changes in expression of *OGG1* mRNA in kidneys of *gpt* delta rats given $KBrO_3$ at a concentration of 500 p.p.m. in their drinking water for 1, 5, 9 and 13 weeks. The values at 0 and 500 p.p.m. in the dose-response study were used as the control and 13-week values, respectively. Means ± SD of data for five rats are given. $^{**}P < 0.01$, significantly different from the controls.

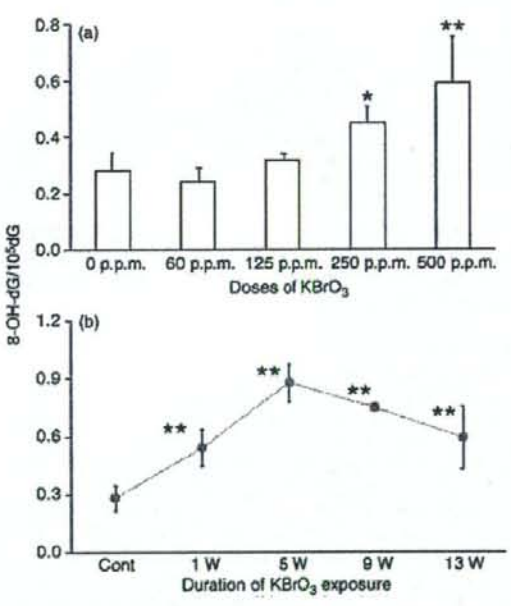

Fig. 2. (a) Dose-dependent induction of 8-OHdG in kidney DNA of *gpt* delta rats given $KBrO_3$ at concentrations of 0, 60, 125, 250 and 500 p.p.m. in their drinking water for 13 weeks. Values are means ± SD of data for five rats. $^*P < 0.01$, $^{**}P < 0.05$, significantly different from the controls (0 p.p.m.). (b) Time course of changes in levels of 8-OHdG in kidneys of *gpt* delta rats given $KBrO_3$ at a concentration of 500 p.p.m. in their drinking water for 1, 5, 9 and 13 weeks. The values at 0 and 500 p.p.m. in the dose-response study were used as the control and 13-week values, respectively. Means ± SD of data for five rats are given. $^{**}P < 0.01$, significantly different from the controls.

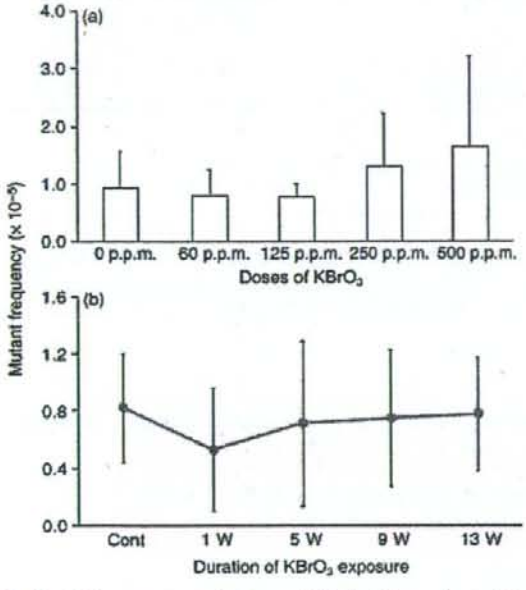

Fig. 3. (a) Dose–response data for *gpt* MFs in kidneys of *gpt* delta rats given $KBrO_3$ at concentrations of 0, 60, 125, 250 and 500 p.p.m. in their drinking water for 13 weeks. Values are means ± SD of data for five rats. (b) Time-course of changes in *gpt* MFs in kidneys of *gpt* delta rats given $KBrO_3$ at a concentration of 500 p.p.m. in their drinking water for 1, 5, 9 and 13 weeks. The values for controls and 13 weeks were obtained from re-analysis of the samples at 0 and 500 p.p.m., respectively, in the dose–response study. Values are means ± SD of data for five rats.

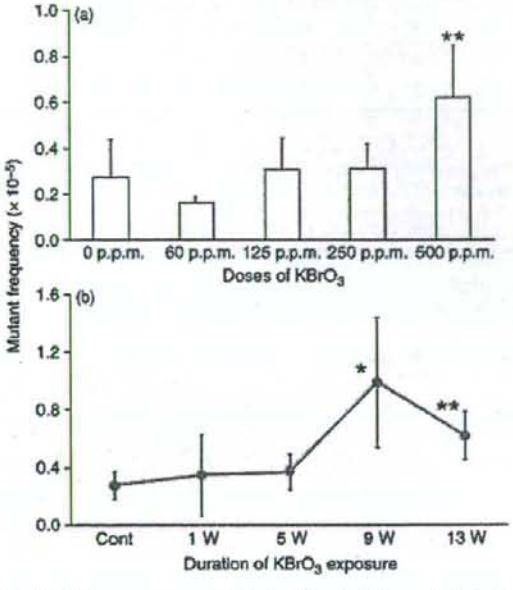

Fig. 4. (a) Dose–response data for Spi^- MFs in kidneys of *gpt* delta rats given $KBrO_3$ at concentrations of 0, 60, 125, 250 and 500 p.p.m. in their drinking water for 13 weeks. Values are means ± SD of data for five rats. $^{**}P < 0.01$, significantly different from the controls (0 p.p.m.). (b) Time-course of changes in Spi^- MFs in kidneys of *gpt* delta rats given $KBrO_3$ at a concentration of 500 p.p.m. in their drinking water for 1, 5, 9 and 13 weeks. The values for the controls and at 13 weeks were obtained from re-analysis of the samples at 0 and 500 p.p.m., respectively, in the dose–response study. Values are means ± SD of data for five rats. $^{*}P < 0.05$, $^{**}P < 0.01$, significantly different from the controls.

treated with 500 p.p.m. $KBrO_3$ was significantly higher ($P < 0.01$) than in untreated control rats (Fig. 4a). As shown in Fig. 4(b), a significant ($P < 0.05$) elevation of Spi^- MF appeared 9 weeks after the start of the exposure.

Experiment II

One animal given $KBrO_3$ at a dose of 250 p.p.m. followed by NTA treatment died of a malignant pheochromocytoma 49 weeks after the start of the experiment and was eliminated from the dataset. Final body weights were 391.3 ± 19.2 g (DW/BD), 3705 ± 23.2 g ($KBrO_3$ 60 p.p.m./NTA), 365.4 ± 18.5 g ($KBrO_3$ 125 p.p.m./NTA), 367.7 ± 26.6 g ($KBrO_3$ 250 p.p.m./NTA), 348.7 ± 20.1 g ($KBrO_3$ 500 p.p.m./NTA, $P < 0.01$ *versus* DW/BD), 360.2 ± 17.0 g (DW/NTA, $P < 0.05$ *versus* DW/BD) and 384.2 ± 18.4 g ($KBrO_3$ 500 p.p.m./BD). The incidences and multiplicities of renal preneoplastic lesions in rats given $KBrO_3$ at various doses for 13 weeks followed by NTA treatment are shown in Table 1. In all of the groups except the no-treatment control group, preneoplastic lesions were found (Fig. 5a,b). The multiplicity ($P < 0.01$) of ATs, and the incidence ($P < 0.05$) and multiplicity ($P < 0.05$) of AHs in rats given $KBrO_3$ at a dose of 500 p.p.m. followed by NTA were significantly elevated as compared with the values for rats given NTA only. A cystic adenoma was observed in a rat given $KBrO_3$ at the dose of 500 p.p.m. for 13 weeks followed by no-treatment for 39 weeks (Fig. 5c). However, there were no neoplastic lesions in any of the other groups.

Discussion

OGG1 mRNA levels have been found to be elevated in rat lungs after exposure to diesel exhaust particles,[6] in rat kidney after ischemic-reperfusion injury,[7] and in human lung alveolar epithelial cells following crocidolite asbestos treatment.[31] Because overexpression in these cases occurred concomitantly with an increment in OGG1 activity, it has been considered that the elevation in *OGG1* gene expression is linked with the increase of OGG1 activity,[31] and formation of 8-OHdG is a trigger for induction of OGG1 activity.[32–34] However, in the present study, overexpression of *OGG1* mRNA in the kidneys of rats given $KBrO_3$ was not demonstrated. It has been reported that OGG1 activities in the kidneys of rats given $KBrO_3$ by single i.p. injection at a dose of 80 mg/kg were increased in a time- and dose-dependent manner.[20] Also, a recent report showed that $KBrO_3$ exposure at a dose of 400 p.p.m. in drinking water for 52 weeks was able to induce an approximately fourfold increase in *OGG1* mRNA expression.[35] Therefore, chronic exposure to $KBrO_3$

doi: 10.1111/j.1349-7006.2006.00248.x

Table 1. Incidence and multiplicity data for preneoplastic lesions in the kidneys of rats given $KBrO_3$ at various doses followed by NTA treatment

Exposure	Number of rats at risk	Atypical tubules		Atypical hyperplasias	
		Incidence (%)	Multiplicity (number/rat)	Incidence (%)	Multiplicity (number/rat)
DW/BD	10	0	0.0	0	0.0
$KBrO_3$ (60 p.p.m)/NTA	15	93	3.1 ± 1.8	27	0.3 ± 0.6
$KBrO_3$ (125 p.p.m)/NTA	15	87	3.0 ± 2.9	27	0.3 ± 0.6
$KBrO_3$ (250 p.p.m)/NTA	14	100	3.7 ± 1.6	36	0.4 ± 0.6
$KBrO_3$ (500 p.p.m)/NTA	15	100	10.1 ± 4.5**	80*	1.3 ± 1.1*
DW/NTA	10	80	2.2 ± 1.5	30	0.4 ± 0.7
$KBrO_3$ (500 p.p.m)/BD	10	50	0.9 ± 1.1	20	0.2 ± 0.4

$KBrO_3$ was given in the drinking water for 13 weeks. NTA was given at a dose of 1% in the diet for 37 weeks. *$P < 0.05$, ** $P < 0.01$ *versus* DW/NTA.

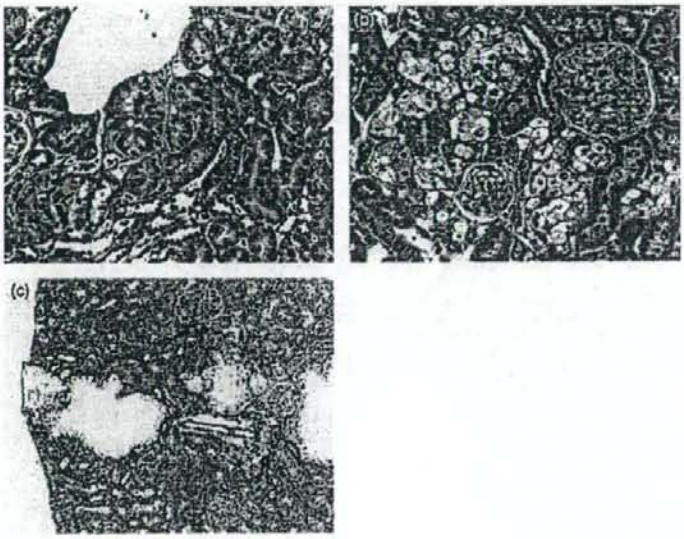

Fig. 5. (a) A single atypical tubule of basophilic cells in a rat treated with KBrO3 at a concentration of 500 p.p.m. in the drinking water for 13 weeks then, after a 2-week rest period, NTA at a concentration of 1% in the diet for 37 weeks. H–E stain. Original magnification × 80. (b) A focus of atypical hyperplasia composed of several atypical tubules, showing a solid structure and clear cell morphology in a rat treated with KBrO3 at a concentration of 500 p.p.m. in the drinking water for 13 weeks then, after a 2-week rest period, NTA at a concentration of 1% in the diet for 37 weeks. H–E stain. Original magnification × 80. (c) Cystic adenoma in a rat treated with $KBrO_3$ at a concentration of 500 pm in the drinking water for 13 weeks followed by no further treatment for 39 weeks. H–E stain. Original magnification × 33.

at carcinogenic levels for 9 weeks might be insufficient for affecting *OGG1* mRNA level.

Even though sustained increases in 8-OHdG formation were apparent through the experimental period, 9 weeks was needed to induce a significant increase of MF. In addition, the MF in the kidneys of rats given $KBrO_3$ at a dose of 250 p.p.m. did not change, despite statistically significant elevated 8-OHdG levels. Accordingly, the present data suggest that a period of time might be necessary for cells having high amounts of 8-OHdG to harbor mutations. This time factor might account for a previous bioassay finding of no initiating effects in rats given $KBrO_3$ by gavage as a single dose of 300 mg/kg, which is sufficient to increase 8-OH-dG levels in kidney DNA, and subsequently subjected to a promoting regimen for 102 weeks.[22]

In the present study, although we failed to detect an increase of *gpt* MF, significant elevation of *red/gam* MF, mainly attributable to deletion mutations, was found. Although it remains uncertain whether the mutation observed in *gpt* delta rats exposed to $KBrO_3$ originates in 8-OHdG, there have been several reports that formation of high amounts of 8-OHdG *in vivo* resulted in several types of mutations, including deletion mutations, besides GC:TA transversions. Previous work with *OGG1* knockout mice demonstrated that surprisingly high amounts of 8-OHdG due to $KBrO_3$ exposure resulted in an increase of deletion mutations and GC:AT transitions as well as GC:TA transversions.[21,36,37] Whereas mutations in NIH3T3 cells transfected with the *ras* gene, which incorporated 8-OHdG at the first position of codon 12, showed mainly GC:TA transversions, incorporation at the second position elicited GC:AT transitions to an appreciable extent.[36,38] Thus, the overall data indicate that mutations other than GC:TA transversions induced by 8-OHdG *in vivo* are possible.[39,40] Additionally, it is highly probable that other oxidized bases, such as 5-formyluracil and 5-hydroxycytosine,[41,42] were generated concomitantly with 8-OHdG formation. The

fact that deletion mutations were predominant among *p15* or *p16* lesions found in renal cell tumors induced by ferric nitrilotriacetate, an agent causing oxidative stress,[43] allows us to speculate that there might be certain types of DNA lesions related to oxidative stress that mainly cause deletion mutations.

The initiation bioassay clearly showed that a 13-week exposure to $KBrO_3$ at 500 p.p.m. was sufficient to induce renal preneoplastic lesions with significant incidence and multiplicity when followed by a typical renal tumor-promoter. Although $KBrO_3$ promotion activity has already been demonstrated in the kidneys of F344 rats when given in their drinking water,[23,44,45] this is the first report showing $KBrO_3$ initiating activity using the two-stage rat renal carcinogenesis model. Because Sprague–Dawley are a back strain of *gpt* delta rats, it seems hard to extrapolate their data to the results obtained from F344 rats. However, in addition to the fact that exposure of F344 rats to $KBrO_3$ at concentrations of 250 and 500 p.p.m. in their drinking water, not at 125 p.p.m. and below, was able to cause increase of 8-OHdG formation,[18] the initiation activity was found in the same dose-dependent fashion as *in vivo* mutagenicity in *gpt* delta rats. Further studies using newly developed *gpt* delta rats of F344 strain are now ongoing. In any case, based on the accumulated data using F344 rats it has been accepted that there is a close link between oxidative DNA damage and $KBrO_3$ carcinogenesis.[46] Considering that the increase of 8-OHdG implies occurrence of intranuclear oxidative stress, the present data suggest that the alteration of the intranuclear circumstances by oxidative stress might have the initiating potential.

In conclusion, the overall data suggest that not only the amount of 8-OHdG but also a period of time with high 8-OHdG levels might be required to bring an oxidized base lesion to mutation status. They also showed a possibility of cells with oxidative DNA damage becoming neoplastic under the influence of an appropriate tumor-promoter.

Acknowledgments

We thank Mss. Machiko Maeda, Ayako Kaneko and Mikiko Takagi for expert technical assistance in carrying out the animal experiments and processing histological materials. This work was supported in part by a Grant-in-Aid for Cancer Research from the Ministry of Health, Labor and Welfare of Japan.

References

1 Kasai H, Nishimura S. Formation of 8-hydroxydeoxyguanosine in DNA by oxygen radicals and its biological significance. In: Sies H. *Oxidative Stress: Oxidants and Antioxidants*. London: Academic Press, 1991; 99–116.
2 Michaels ML, Pham L, Cruz C, Miller JH. MutM, a protein that prevents G.C.-T.A. transversions, is formamidopyrimidine-DNA glycosylase. *Nucleic Acids Res* 1991; **19**: 3629–32.
3 Aburatani H, Hippo Y, Ishida T *et al.* Cloning and characterization of mammalian 8-hydroxyguanine-specific DNA glycosylase/apurinic, apyrimidic lyase, a function mutM homologue. *Cancer Res* 1997; **57**: 2151–6.
4 Zharkov DO, Grollman AP. MutY DNA glycosylase: base release and intermediate complex formation. *Biochemistry* 1998; **37**: 12384–94.
5 Fujikawa K, Kamiya H, Yakushiji H, Fujii Y, Nakabeppu Y, Kasai H. The oxidized forms of dATP are substrates for the human MutT homologue, the hMTHi protein. *J Biol Chem* 1999; **274**: 18201–5.
6 Tsurudome Y, Hirano T, Yamamoto H *et al.* Changes in levels of 8-hydroxyguanine in DNA, its repair and *OGG1* mRNA in rat lungs after intratracheal administration of diesel exhaust particles. *Carcinogenesis* 1999; **20**: 1573–6.
7 Tsuruya K, Furuichi M, Tominaga Y *et al.* Accumulation of 8-oxoguanine in the cellular DNA and the alteration of the *OGG1* expression during ischemic-reperfusion injury in the rat kidney. *DNA Repair* 2003; **2**: 211–29.
8 Yamaguchi R, Hirano T, Asami S, Chung M-H, Sugita A, Kasai H. Increased 8-hydroxyguanine levels in DNA and its repair activity in rat kidney after administration of a renal carcinogen, ferric nitrilotriacetate. *Carcinogenesis* 1996; **17**: 2419–22.
9 Lee M-R, Kim S-H, Cho H-J *et al.* Transcription factors NF-YA regulate the induction of human OGG1 following DNA-alkylating agent methylmethane sulfonate (MMS) treatment. *J Biol Chem* 2004; **279**: 9857–66.
10 Kurokawa Y, Hayashi Y, Maekawa A, Takahashi M, Kokubo T. Induction of renal tumors in F344 rats by oral administration of potassium bromate, a food additive. *Jpn J Cancer Res* 1982; **73**: 335–8.
11 Ishidate M, Sofuni T, Yoshioka K *et al.* Primary mutagenicity screening of food additives currently used in Japan. *Food Chem Toxicol* 1984; **22**: 623–36.
12 Ishidate M, Yoshioka K. Chromosome aberration tests with Chinese hamster cells *in vitro* with and without metabolic activation: a comparative study on mutagens and carcinogens. *Arch Toxicol Supplement* 1980; **4**: 41–4.
13 Hayashi M, Kishi M, Sofuni T, Ishidate M. Micronucleus tests with mice on 39 food additives and 8 miscellaneous chemical substances. *Chem Toxicol* 1988; **26**: 487–500.
14 Sai K, Uchiyama S, Ohno Y, Hasegawa R, Kurokawa Y. Generation of active oxygen species *in vitro* by the interaction of potassium bromate with rat kidney cells. *Carcinogenesis* 1992; **13**: 333–9.
15 Sai K, Takagi A, Umemura T, Hasegawa R, Kurokawa Y. The protective role of glutathione, cysteine and vitamin C against oxidative DNA damage induced in rat kidney by potassium bromate. *Jpn J Cancer Res* 1992; **83**: 45–51.
16 Ballmaier D, Epe B. Oxidative DNA damage induced by potassium bromate under cell-free conditions and in mammalian cells. *Carcinogenesis* 1995; **16**: 335–42.
17 Kasai H, Nishimura S, Kurokawa Y, Hayashi Y. Oral administration of the renal carcinogen, potassium bromate, specifically produces 8-hydroxydeoxyguanosine in rat kidney target organ DNA. *Carcinogenesis* 1987; **8**: 1959–61.
18 Umemura T, Kitamura Y, Kanki K *et al.* Dose-related changes of oxidative stress and cell proliferation in kidneys of male and female F344 rats exposed to potassium bromate. *Cancer Sci* 2004; **95**: 393–8.
19 Umemura T, Sai K, Takagi A, Hasegawa R, Kurokawa Y. A possible role for cell proliferation in potassium bromate ($KBrO_3$) carcinogenesis. *J Cancer Res Clin Oncol* 1993; **119**: 463–9.
20 Lee Y-S, Choi J-Y, Park M-K, Choi E-M, Kasai H, Chung M-H. Induction of oh8Gua glycosylase in rat kidneys by potassium bromate ($KBrO_3$), a renal oxidative carcinogen. *Mutat Res* 1996; **364**: 227–33.
21 Arai T, Kelly VP, Minowa O, Noda T, Nishimura S. High accumulation of oxidative DNA damage, 8-hydroxyguanine, in *Mmh/OGG1* deficient mice by chronic oxidative stress. *Carcinogenesis* 2002; **23**: 2005–10.
22 Kurata Y, Diwan BA, Ward JM. Lack of renal tumor initiating activity of a single dose of potassium bromate, a genotoxic renal carcinogen in male F344/NCr rats. *Food Chem Toxicol* 1992; **30**: 251–9.
23 Kurokawa Y, Maekawa A, Takahashi M, Hayashi Y. Toxicity and carcinogenicity of potassium bromate – a new renal carcinogen. *Environ Health Perspect* 1990; **87**: 309–35.
24 Hiasa Y, Kitahori Y, Konishi N, Shimoyama T. Dose-related effect of trisodium nitriloacetate monohydrate on renal tumorigenesis initiated with *N*-ethyl-*N*-hydroxyethyl-nitrosamine in rats. *Carcinogenesis* 1985; **6**: 907–10.
25 Nagata M, Fujita H, Ida H *et al.* Identification of potential biomarkers of lymph node metastasis in oral squamous cell carcinoma by cDNA microarray analysis. *Int J Cancer* 2003; **106**: 683–9.
26 Kasai H. Chemistry-based studies on oxidative DNA damage: formation, repair, and mutagenesis. *Free Rad Biol Med* 2002; **33**: 450–6.
27 Nakae D, Mizumoto Y, Kobayashi E, Noguchi O, Konishi Y. Improved genomic/nuclear DNA extraction for 8-hydroxydeoxyguanosine analysis of small amounts of rat liver tissue. *Cancer Lett* 1995; **97**: 233–9.
28 Helbock HJ, Beckman KB, Shigenaga MK *et al.* DNA oxidation matters:

doi: 10.1111/j.1349-7006.2006.00248.x

the HPLC-electrochemical detection assay of 8-oxo-deoxyguanosine and 8-oxo-guanine. *Proc Natl Acad Sci USA* 1998; **95**: 288–93.
29 Kanki K, Nishikawa A, Masumura K *et al. In vivo* mutational analysis of liver DNA in *gpt* delta transgenic rats treated with the hepatocarcinogens *N*-nitrosopyrrolidine, 2-amino-3-methylimidazo[4,5-*f*]quinoline, and di(2-ethylhexyl)phthalate. *Mol Carcinog* 2005; **42**: 9–17.
30 Dietrich DR, Swenberg JA. Preneoplastic lesions in rodent kidney induced spontaneously or by non-genotoxic agents: predictive nature and comparison to lesions induced by genotoxic carcinogens. *Mutat Res* 1991; **248**: 239–60.
31 Kim H-N, Morimoto Y, Tsuda T *et al.* Changes in DNA 8-hydroxyguanine levels, 8-hydroxyguanine repair activity, and *hOGG1* and *hMTH1* mRNA expression in human lung alveolar epithelial cells induced by crocidolite asbestos. *Carcinogenesis* 2001; **22**: 265–9.
32 Hollenbach S, Dhenaut A, Eckert I, Radicella JP, Epe B. Overexpression of OGG1 in mammalian cells: effects on induced and spontaneous oxidative DNA damage and mutagenesis. *Carcinogenesis* 1999; **20**: 1863–8.
33 Bruner SD, Norman DPG, Verdine GL. Structural basis for recognition and repair of the endogenous mutagen 8-oxoguanine in DNA. *Nature* 2000; **403**: 859–66.
34 Kuznetsov NA, Koval VV, Zharkov DO, Nevinsky GA, Douglas KT, Fedorova OS. Kinetics of substrate recognition and cleavage by human 8-oxoguanine-DNA glycosylase. *Nucleic Acids Res* 2005; **33**: 3919–31.
35 Delker D, Hatch G, Allen J *et al.* Molecular biomarkers of oxidative stress associated with bromated carcinogenicity. *Toxicology* 2006; **221**: 158–65.
36 Nishimura S. Involvement of mammalian OGG1 (MMH) in excision of the 8-hydroxyguanine residue in DNA. *Free Rad Biol Med* 2002; **32**: 813–21.
37 Arai T, Kelly VP, Komoro K, Minowa O, Noda T, Nishimura S. Cell proliferation in liver of *Mmh/Ogg1*-deficient mice enhances mutation frequency because of the presence of 8-hydroxyguanine in DNA. *Cancer Res* 2003; **63**: 4287–92.
38 Kamiya H, Murata-Kamiya N, Koizume S, Inoue H, Nishimura S, Ohtsuka E. 8-Hydroxyguanine (7,8-dihydro-8-oxoguanine) in hot spots of the c-Ha-*ras* gene: effects of sequence contexts on mutation spectra. *Carcinogenesis* 1995; **16**: 883–9.
39 Jaloszynski P, Masutani C, Hanaoka F, Perez AB, Nishimura S. 8-Hydroxyguanine in a mutational hotspot of the c-Ha-*ras* gene causes misreplication, 'action-at-a-distance' mutagenesis and inhibition of replication. *Nucleic Acids Res* 2003; **31**: 6085–95.
40 Dybdahl M, Risom L, Moller P *et al.* DNA adduct formation and oxidative stress in colon and liver Big Blue rats after dietary exposure to diesel particles. *Carcinogenesis* 2003; **24**: 1759–66.
41 Fujikawa K, Kamiya H, Kasai H. The mutations induced by oxidatively damaged nucleotides, 5-formyl-dUTP and 5-hydroxy-dCTP, in Escherichia coli. *Nucleic Acids Res* 1998; **26**: 4582–7.
42 Wallace SS. Biological consequences of free radical-damaged DNA bases. *Free Rad Biol Med* 2002; **33**: 1–14.
43 Tanaka T, Iwasa Y, Kondo S, Hiai H, Toyokuni S. High incidence of allelic loss on chromosome 5 and inactivation of $p15^{INK4B}$ and $p16^{INK4A}$ tumor suppressor genes in oxystress-induced renal cell carcinoma of rats. *Oncogene* 1999; **18**: 3793–7.
44 Umemura T, Takagi A, Sai K, Hasegawa R, Kurokawa Y. Oxidative DNA damage and cell proliferation in kidneys of male and female rats during 13-weeks exposure to potassium bromate ($KBrO_3$). *Arch Toxicol* 1998; **72**: 264–9.
45 Umemura T, Sai K, Takagi A, Hasegawa R, Kurokawa Y. A possible role for oxidative stress in $KBrO_3$ carcinogenesis. *Carcinogenesis* 1995; **16**: 593–7.
46 Umemura T, Kurokawa Y. Etiology of bromated-induced cancer and possible modes of action-studies in Japan. *Toxicology* 2006; **221**: 154–7.

Available online at www.sciencedirect.com
ScienceDirect
Mutation Research 609 (2006) 102–115
Genetic Toxicology and Environmental Mutagenesis
www.elsevier.com/locate/gentox
Community address: www.elsevier.com/locate/mutres

A newly established GDL1 cell line from *gpt* delta mice well reflects the in vivo mutation spectra induced by mitomycin C

Akira Takeiri[a,*], Masayuki Mishima[a], Kenji Tanaka[a], Akifumi Shioda[a], Asako Harada[a], Kazuto Watanabe[a], Ken-Ichi Masumura[b], Takehiko Nohmi[b]

[a] *Fuji Gotemba Research Laboratories, Chugai Pharmaceutical Co. Ltd., 1-135 Komakado, Gotemba, Shizuoka 412-8513, Japan*
[b] *Division of Genetics and Mutagenesis, National Institute of Health Sciences, 1-18-1 Kamiyoga, Setagaya, Tokyo 158-8501, Japan*

Received 8 May 2006; received in revised form 19 June 2006; accepted 30 June 2006
Available online 17 August 2006

Abstract

In order to create a novel in vitro test system for detection of large deletions and point mutations, we developed an immortalized cell line. A SV40 large T antigen expression unit was introduced into fibroblasts derived from *gpt* delta mouse lung tissue and a selected clone was established as the *gpt* delta L1 (GDL1) cell line. The novel GDL1 cells were examined for mutant frequencies (MFs) and for molecular characterization of mutations induced by mitomycin C (MMC). The GDL1 cells were treated with MMC at doses of 0.025, 0.05, and 0.1 μg/mL for 24 h and mutations were detected by Spi$^-$ and 6-thioguanine (6-TG) selections. The MFs of the MMC-treated cells increased up to 3.4-fold with Spi$^-$ selection and 3.5-fold with 6-TG selection compared to MFs of untreated cells. In the Spi$^-$ mutants, the number of large (up to 76 kilo base pair (kbp)) deletion mutations increased. A majority of the large deletion mutations had 1–4 base pairs (bp) of microhomology in the deletion junctions. A number of the rearranged deletion mutations were accompanied with deletions and insertions of up to 1.1 kbp. In the *gpt* mutants obtained from 6-TG selection, single base substitutions of G:C to T:A, tandem base substitutions occurring at the 5′-GG-3′ or 5′-CG-3′ sequence, and deletion mutations larger than 2 bp were increased. We compared the spectrum of MMC-induced mutations observed in vitro to that of in vivo using *gpt* delta mice, which we reported previously. Although a slight difference was observed in MMC-induced mutation spectra between in vitro and in vivo, the mutations detected in vitro included all of the types of mutations observed in vivo. The present study demonstrates that the newly established GDL1 cell line is a useful tool to detect and analyze various mutations including large deletions in mammalian cells.

Keywords: Mitomycin C; Cell line; *gpt* delta mice

1. Introduction

Point mutations and deletion mutations are major genotoxic events induced by chemicals and ionizing radiation. In particular, deletion mutations constitute an important class of mutations that may result in a variety of human diseases including cancer [1]. Development of various in vivo test systems suitable for detection and analysis of point mutations have provided a better understanding of molecular properties of chemical mutagenesis [2,3]. However, fewer methodologies are available to analyze deletion mutations compared with

* Corresponding author. Tel.: +81 550 87 6376; fax: +81 550 87 6383.
E-mail address: takeiriakr@chugai-pharm.co.jp (A. Takeiri).

1383-5718/$ – see front matter © 2006 Elsevier B.V. All rights reserved.
doi:10.1016/j.mrgentox.2006.06.026

point mutations. Recently, successful and convenient approaches for the analysis of deletion mutations using transgenic (TG) animal models have been constructed [4,5]. The *lacZ* plasmid-based TG mouse assay detects deletion mutations induced by X-ray and cisplatin [5,6]. The *gpt* delta mice efficiently detects deletion mutations induced by various mutagens, e.g., mitomycin C (MMC) [7,8], heavy-ion, X-ray [9], gamma-ray [9,10], and ultraviolet B [11,12]. In the *gpt* delta mice, approximately 80 copies of the lambda EG10 shuttle vector DNA carrying the *red/gam* genes of lambda phage and the *gpt* gene of *Escherichia coli* are integrated into this TG mouse on chromosome 17 of the C57BL/6J background [2,4]. Deletion mutations in the *red/gam* genes and point mutations in the *gpt* gene can be individually identified by Spi^- (sensitive to P2 interference) selection and 6-thioguanine (6-TG) selection, respectively [2].

MMC is a natural cytotoxic and genotoxic agent used in clinical anticancer chemotherapy [13]. The mode of action of this agent in mutagenicity is intriguing and well investigated. MMC alkylates DNA in several different ways [14]. It binds to the N^2 position of guanine in DNA and forms monoalkylation products. Furthermore, after the carbamate at C-10″ is lost, it will give rise to another active site capable of alkylating the second guanine within the DNA. Alkylation of two guanine bases on the same DNA strand results in the formation of intrastrand cross-links within the 5′-GG-3′ sequence, and the alkylation of guanine bases on opposite DNA strands leads to the formation of interstrand cross-links within the 5′-CG-3′ sequence [15–19]. Interaction of MMC and DNA strands causes the production of characteristic mutations. In our previous in vivo study, MMC-induced tandem base substitutions and deletion mutations up to about 8 kilo base pair (kbp) in size [8].

Since it is often advantageous to use in vitro test systems in mechanistic investigations, we newly established the GDL1 cell line harboring the same reporter gene system as *gpt* delta mice. The cells were established from lung fibroblasts of the *gpt* delta mice with a functional reduction of p53 protein by intracellular expression of the Simian virus 40 large T antigen (SV40 T antigen). GDL1 was exposed to MMC to characterize the induced mutations. Comparing the results from GDL1 cells with those previously reported in vivo, there was little difference in mutation spectra and all of the types of mutations in vivo were involved in the events detected with GDL1 cells. The GDL1 cell is a novel tool available for molecular analysis of deletion mutations. Furthermore, we here discuss the contribution of the dysfunction of p53 by the SV40 T antigen to the differences between the MMC-induced mutations in the GDL1 cells and in the *gpt* delta mice.

2. Materials and methods

2.1. Collection of the fibroblasts

Lung tissues were obtained from 21-week-old female *gpt* delta mice maintained in our laboratory. The tissues were minced in Eagle's minimum essential medium (MEM, Sigma–Aldrich, St. Louis, MO, USA) and trypsinized in MEM including 0.1% (w/v) trypsin, 0.01% (w/v) EDTA for 1 h at 37 °C. After centrifugation, the down pellet containing fibroblast cells was suspended in Dulbecco's modified Eagle's medium (DMEM, Sigma–Aldrich, St. Louis, MO, USA) including 10% (v/v) fetal bovine serum (FBS, Invitrogen, Carlsbad, CA, USA). The cells were cultured in 75-cm^2 culture flasks (BD Biosciences, Franklin Lakes, NJ, USA) in an atmosphere of 5% CO_2 at 37 °C.

2.2. Establishment of the cell line

A plasmid encoding the complete sequence for the SV40 T antigen was obtained from the Health Science Research Resources Bank (Osaka, Japan): pMTIOD, registration no. VG026 [20]. The complete sequence of the T antigen gene was excised from pMTIOD and inserted into an expression vector at the downstream of the elongation factor 1 alpha promoter, resulting in pCOSV1. The constructed vector was introduced into the fibroblasts using a lipofection reagent, FuGENE6 (Roche Diagnostics, Tokyo, Japan). The transfectants were selected by culture in DMEM containing 100 μg/mL of G-418 for 1 week. The cells were cloned and, after approximately 60 passages in DMEM supplemented with 10% (v/v) FBS in an atmosphere of 5% CO_2 at 37 °C, we selected a stably growing single clone (clone #2) to establish the GDL1 cell.

2.3. Measurement of chromosome number and immunostaining

A single cloned GDL1 cell stock frozen in liquid nitrogen was thawed and maintained in DMEM supplemented with 10% (v/v) FBS in an atmosphere of 5% CO_2 at 37 °C. For measurement of chromosome number, the cells were treated with 0.1 μg/mL colcemid (Wako Pure Chemical Industries, Osaka, Japan) for 2 h. The trypsinized cells using PBS including 0.1% (w/v) trypsin, 0.01% (w/v) EDTA were suspended in 75 mM KCl hypotonic solution and fixed with acetic acid and methanol (1:3) mixture. The cell suspensions were dropped on glass slides and dried. The metaphase spreads of the cells were stained with Giemsa and each chromosome of 100 metaphases was scored. The cells cultured in a 24-well culture plate (BD Biosciences, Franklin Lakes, NJ, USA) were fixed by 99.5% methanol and then examined for SV40 T antigen expression by immunofluorescent assay. The cells were stained with anti-

SV40 large T monoclonal antibody, SV40T-Ag (Ab-2) (EMD Biosciences, San Diego, CA, USA), and FITC conjugated anti-mouse immunoglobulin polyclonal antibody (Dako Cytomation, Carpinteria, CA, USA).

2.4. Cytotoxicity

GDL1 cells were seeded in 12-multiwell culture plate (Corning, Corning, NY, USA) at a density of 4×10^4 cells/mL in each well. One day after the seeding, the cells were treated with mitomycin C (MMC, CAS no. 50-07-7, Kyowa Hakko Kogyo, Tokyo, Japan) at doses of 0.025, 0.05, and 0.1 μg/mL for 24 h. The solutions of chemicals were freshly prepared at 100-fold of final concentration in saline. The cells were trypsinized and resuspended in DMEM supplemented with 10% (v/v) FBS. The number of cells was counted using automated hematology analyzer KX-21 (Sysmex, Kobe, Japan).

2.5. Treatment with MMC and preparation of lambda EG10 phage

GDL1 cells were subcultured and divided into flasks for chemical treatment at 1×10^5 cells/5 mL medium per 25-cm^2 culture flask 2 days before the treatment. Three culture flasks were prepared for each dose of MMC and untreated control. The cells were exposed to MMC at doses of 0.025, 0.05, or 0.1 μg/mL for 24 h, washed, and cultured for an additional 6 days. The additional 6 days is considered sufficient for fixation of mutations [21]. During the 6-day culture, the cells were subcultured two times; the culture volume was increased to 10 mL and transferred to 75-cm^2 culture flasks. DNA samples of the cells were prepared using a RecoverEase DNA isolation kit (Stratagene, La Jolla, CA, USA). The lambda EG10 phages were rescued from the DNA by in vitro packaging reaction using Transpack packaging extract (Stratagene, La Jolla, CA, USA) according to the manufacturer's instruction.

2.6. Measurement of mutant frequency (MF) and sequence analysis

The Spi$^-$ mutation assay was performed as described previously [2,10,12]. The rescued phages were infected to *E. coli* XL1-Blue MRA (P2) (Stratagene, La Jolla, CA, USA). The infected host cells were poured onto lambda-trypticase agar plates and incubated at 37 °C to detect mutant phage plaque. The rescued phages were diluted and infected to *E. coli* XL1-Blue MRA (Stratagene, La Jolla, CA, USA) to determine total number of phage plaques. The Spi$^-$ MF was calculated as previously reported [2,10,12]. The entire sequence of lambda EG10 phage and the detail method of Spi$^-$ selection and 6-TG selection is available at: http://www.dgm2alpha.nihs.go.jp/dgm2/.

The *gpt* mutagenesis assay was performed according to previous method [2,11]. Briefly, the lambda EG10 phages were converted to plasmids by the infection to *E. coli* YG6020 which was expressing Cre recombinase. The infected bacteria were poured onto agar plates containing chloramphenicol (Cm) and 6-TG. The plates were incubated at 37 °C for the selection of colonies harboring plasmids carrying the mutated *gpt* gene. The infected host bacteria were diluted and poured on the plates containing Cm alone to determine the total number of rescued plasmids. The *gpt* MF was calculated as previously reported [2,11].

In the cells treated with 0.1 μg/mL MMC or untreated, the Spi$^-$ mutants and *gpt* mutants obtained from Spi$^-$ selection and 6-TG selection, respectively, were used for sequence analysis as previously described [2,8,10–12]. The sequences of the *gam* gene or DNA sequences surrounding the deletion junction were analyzed in 43 Spi$^-$ mutants from untreated cells and 45 mutants from MMC-treated cells. Forty-five *gpt* mutants each from untreated and MMC-treated cells were analyzed. In Spi$^-$ mutants and *gpt* mutants, the mutations analyzed were classified by the types of mutation. The ratio of each type of mutation to total mutation was multiplied by total MF for calculation of specific MF. The specific MFs of the MMC-treated cells were statistically compared to those of the control cells using Fisher's exact test according to the method of Carr and Gorelick [22].

3. Results

3.1. Induction of Spi$^-$ and gpt mutations by MMC in GDL1 cells

We established the GDL1 cell line from fibroblasts of the lung of *gpt* delta TG mice by introduction of plasmid pCOSV1 expressing SV40 T antigen. The doubling time of the cell line was approximately 12 h (data not shown), and the cells were polyploid with a modal chromosome number of 74 ($2N = 40$ in mice) (Fig. 1). SV40 T antigen was expressed and localized in the nucleus (data not shown). To characterize the GDL1 cell line as a tester for genotoxicity assays, we examined the Spi$^-$ and *gpt* mutations induced by MMC at the molecular

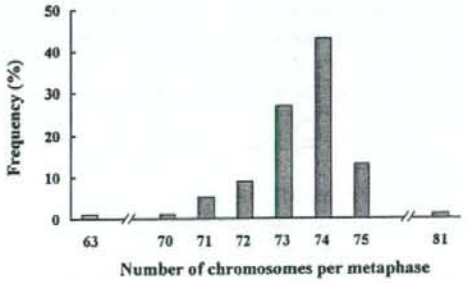

Fig. 1. Chromosome frequency distribution in GDL1 cells. The number of chromosomes in a spread of 100 metaphase cells was calculated. The modal chromosome number was 74 ($2N = 40$ in mice).

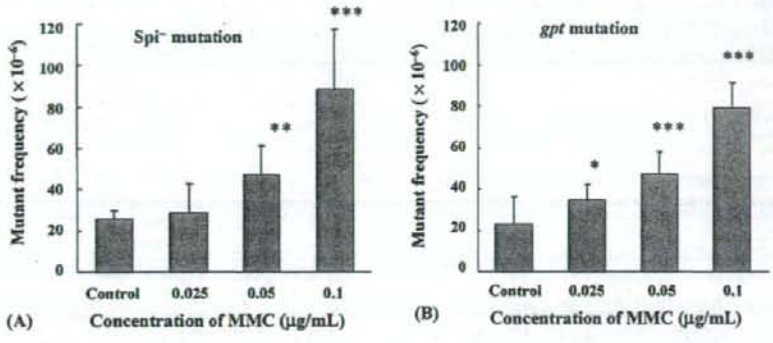

Fig. 2. Mutant frequencies in MMC-treated GDL1 cells. (A) Spi⁻ mutant frequencies; (B) *gpt* mutant frequencies. Cells were treated with MMC at the doses of 0.025, 0.05, and 0.1 μg/mL for 24 h. After a 6-day culture, the cells were harvested. As the control, untreated cells were collected after a 6-day cell culture. Spi⁻ mutant frequency in Spi⁻ selection and *gpt* mutant frequency in 6-TG selection were determined. *P* values calculated by Fisher's exact test were $P < 0.05$ (*), $P < 0.001$ (**), and $P < 0.0001$ (***). Bars represent mean and standard deviations of data obtained from three independent cell culture flasks.

level. In the MMC-treated group, Spi⁻ MFs at concentrations of 0.025, 0.05, and 0.1 μg/mL were 28.4×10^{-6}, 47.0×10^{-6}, and 88.0×10^{-6}, respectively (Fig. 2A). MFs increased in a dose-dependent manner up to 3.4 times higher than the control group, i.e., 25.6×10^{-6}. On the other hand, *gpt* MFs at concentrations of 0.025, 0.05, and 0.1 μg/mL were 34.8×10^{-6}, 47.0×10^{-6}, and 78.9×10^{-6}, respectively (Fig. 2B). The *gpt* MFs increased in a dose-dependent manner up to 3.5-fold compared with the control group, i.e., 22.7×10^{-6}. The numbers of cells treated with MMC for 24 h were 73, 53, and 40% of untreated cells in 0.025, 0.05, and 0.1 μg/mL of MMC, respectively.

3.2. Molecular nature of Spi⁻ mutations induced by MMC

To characterize the molecular nature of Spi⁻ mutations induced by MMC, we sequenced 43 and 45 Spi⁻ mutants from untreated cells and cells treated with MMC (0.1 μg/mL), respectively, and categorized them into five classes (Table 1). The specific MF for each class and subclass was determined by multiplying the percentage of each class of mutants and the total MF, and the calculated values were compared between untreated and treated groups.

Large deletions more than 1 kbp in deletion size were classified as class I. They were subclassified into classes I-A and I-B depending on the existence of homologous sequences at the junctions. The specific MF class I-A, i.e., large deletion with short homology (microhomology) at the junction, was enhanced more than four-fold by treatments with MMC (17.6×10^{-6} versus 4.2×10^{-6}, Table 1). The deletion sizes of nine class I-A mutants from the MMC-treated group were from 3829 to 7178 base pair (bp) (Fig. 3). They were all unique in size and position of the deletions. In addition, three class I-B mutants, i.e., large deletions without short homologous sequence, were identified in the treated group. Two of them were simple deletion mutants with deletion sizes of 3345 and 5204 bp, but one mutant, sM2-3, had an insertion of 16 bp with a deletion size of 5676 bp (Fig. 3). In contrast, class I mutants of the untreated group were all class I-A and no class I-B mutants were identified. Five of seven class I-A mutants from untreated cells were completely the same in size and position of deletions (Fig. 3). Since they were independently identified in the mutants and derived from independent culture flasks, they might have been generated by hot spot mutations in untreated GDL1 cells. Alternatively, the mutation might have occurred prior to the subculture of the cells for untreated groups (clonally expanded mutants). The deletion sizes of the seven class I-A mutants were from 3308 to 6827 bp.

Midsized deletions with sizes of from 2 bp to 1 kbp were classified as class II. The specific MF for class II was enhanced more than six times by the treatments with MMC (7.8×10^{-6} versus 1.2×10^{-6}, Table 1). The deletion sizes of four mutants in the MMC-treated group were from 9 to 129 bp (Fig. 3). They were all unique in size and position of the deletions. Two of them were simple deletion mutants with deletion sizes of 9 and 129 bp, and the deleted regions were flanked by two short homologous sequences. Other two deletions had flush ends but had insertions of 9 and 8 bp in the junctions. The deleted sequences were enclosed by short repetitive sequences.

Table 1
Summary of Spi⁻ mutations derived from the GDL1 cells

Type of mutation	Class of mutation	Control		MMC		P value[a]
		No. of mutants (%)	Specific MF[b] ($\times 10^{-6}$)	No. of mutants (%)	Specific MF[b] ($\times 10^{-6}$)	
Large deletion (>1 kbp)						
With microhomology	I-A	7 (16.3)	4.2	9 (20.0)	17.6	<0.01
Without microhomology	I-B	0 (0.0)	0.0	3 (6.7)	5.9	<0.05
Midsize deletion (2 bp to 1 kbp)	II	2 (4.7)	1.2	4 (8.9)	7.8	<0.05
Single base deletion						
At run sequence	III-A	29 (67.4)	17.3	17 (37.8)	33.2	0.06
At non-run sequence	III-B	2 (4.7)	1.2	0 (0.0)	0.0	1.00
Complex mutation	IV	0 (0.0)	0.0	5 (11.1)	9.8	<0.001
Miscellaneous mutation	V					
Transversion						
G:C → T:A		2 (4.7)	1.2	0 (0.0)	0.0	1.00
A:T → T:A		0 (0.0)	0.0	2 (4.4)	3.9	0.06
Tandem base substitution						
GG:CC → TA:AT		0 (0.0)	0.0	1 (2.2)	2.0	0.24
GG:CC → TT:AA		0 (0.0)	0.0	1 (2.2)	2.0	0.24
Other substitution		1 (2.3)	0.6	2 (4.4)	3.9	0.15
Unidentified		0 (0.0)	0.0	1 (2.2)	2.0	0.24
Total		43 (100)	25.6	45 (100)	88.0	<0.0001

[a] *P* values were determined using Fisher's exact test according to Carr and Gorelick [22].
[b] Specific MF was calculated by multiplying the total mutation frequency by the ratio of each type of mutation to the total mutation.

In the control group, two of the class II mutations were simple deletions with sizes of 13 and 206 bp.

Single base deletions occurring in the *gam* gene were classified as class III with subclasses of classes III-A and III-B. Single base deletion induced at a run sequence of identical bases, e.g., −1A deletion at 5′-AAAAAA-3′ of nucleotides 295–300 (Fig. 4), were classified as class III-A and single base deletions occurring at a non-run sequence were classified as class III-B. The specific MF of class III-A was enhanced about two times by the MMC treatments (33.2×10^{-6} versus 17.3×10^{-6}, Table 1). The class III-A was dominant over III-B in both MMC-treated and control groups.

Complex mutations were classified as class IV. Five mutants of this class were observed in the MMC-treated group, while no such mutants were observed in the control group. All five MMC-induced class IV mutations were deletions with complex rearrangements (Figs. 3 and 5). Mutant sM1-9, with a deleted region of approximately 5 kbp, had an inserted fragment larger than 1 kbp, which was homologous to the sequence in chromosome 16 of mouse from the DNA data base (http://www.ddbj.nig.ac.jp/). Since the lambda EG10 DNA is integrated in chromosome 17 of the *gpt* delta mouse, the mutation was due to inter-chromosomal translocation. In mutant sM2-6, a 7632 bp region including the *red/gam* genes was deleted, and three DNA fragments derived from the deleted region – fragment 1 (457 bp), fragment 2 (153 bp), and fragment 3 (1115 bp) – were incorrectly inserted again. In mutant sM2-12, a region of 3459 bp was deleted and a fragment of 403 bp, which was located at approximately 1.2 kbp from the deleted site, was inserted into the deletion site. In mutant sM2-14, the deletion size was approximately 5 kbp. A sequence existing approximately 6 kbp away from the deletion site was inserted into the deletion junction in the opposite direction. The accurate size of the inserted fragment was not determined. In mutant sM3-7, the deletion size determined by agarose-gel electrophoresis of the PCR product was approximately 5 kbp. A DNA fragment located approximately 18 kbp away from the deletion site was inserted into the deletion site. The size of the inserted fragment could not be determined accurately. Almost all of the deletion junctions observed in the complex rearrangements mentioned above had microhomology sequences (Fig. 3).

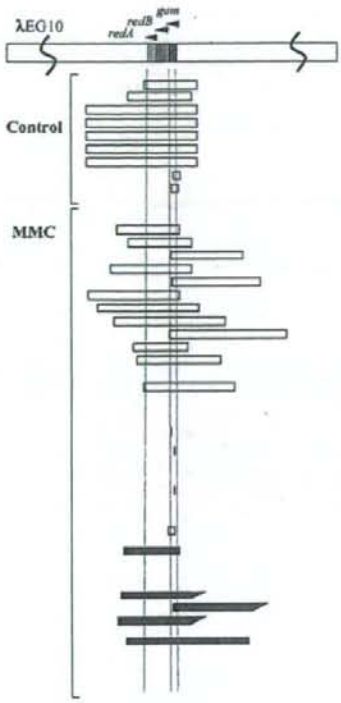

Treatment	Mutant code	Class	Mutation	Sequence of deletion junction
Control	sC3- 3	I-A	-3,308 bp deletion	TCCCTGGTGTTCACAT TCATCTGTTGAGTTA
	sC2- 1	I-A	-3,979 bp deletion	TTATTGAAAAACAAA TAAACTGGAAAGCAA
	sC1- 8	I-A	-4,827 bp deletion	TTGTTTTACTGCGGG GATGAATCCGTCAGT
	sC1- 9	I-A	-4,827 bp deletion	TTGTTTTACTGCGGG GATGAATCCGTCAGT
	sC2- 7	I-A	-4,827 bp deletion	TTGTTTTCTGCGGG GATGAATCCGTCAGT
	sC3- 9	I-A	-4,827 bp deletion	TTGTTTTACTGCGGG GATGAATCCGTCAGT
	sC3- 10	I-A	-4,827 bp deletion	TTGTTTTACTGCGGG GATGAATCCGTCAGT
	sC1- 2	II	-13 bp deletion	CGTCACTACCAGCAG AGAGAAACAGCACA
	sC3- 11	II	-206 bp deletion	CTAATCAGCCCGGCA ACCGGGCCAGCAAAA
MMC 0.1 μg/mL	sM1- 7	I-A	-3,829 bp deletion	GATGTTTCGTGAAGC CGGTGGAAACGATAC
	sM1- 10	I-A	-3,979 bp deletion	TTATTGAAAAACAAA TAAACTGGAAAGCAA
	sM1- 12	I-A	-4,424 bp deletion	TGCAGGATATCGACC ACCATTGCTCACCAC
	sM3- 12	I-A	-4,996 bp deletion	CTACCAAACAATGCC GCCTTGAAACAGTTC
	sM3- 11	I-A	-5,454 bp deletion	ACGCGGCGCTCGATG GATGACGATGTTGAG
	sM2- 9	I-A	-5,618 bp deletion	CTAACCCCCTTTCCT CTTTACTGCCATATT
	sM2- 15	I-A	-6,230 bp deletion	TGCAGGAACGATGAT GATATCTTTATGTCG
	sM3- 15	I-A	-6,822 bp deletion	AGGAACAACTGCCGG GGAGAATGGAATGGA
	sM1- 15	I-A	-7,178 bp deletion	ATGATAACCATTGCG CGTGTCGGCATGGAT
	sM3- 13	I-B	-3,345 bp deletion	AAGGCTTTGGGGTGT ACGCCTGGTCGTTCA
	sM3- 1	I-B	-5,204 bp deletion	GGAGAGATCCCCTGGC GCAGCTACAGGCTCC
	sM2- 3	I-B	-5,676 bp deletion, +16 bp insertion	TTTTTACCGCCAGAT AGCCGCATCCCTTTC ^ AATGGTCTGCGCTTGA
	sM3- 4	II	-9 bp deletion	CATGGCAGAACACAT ATGGTTGAAACCATT
	sM3- 10	II	-13 bp deletion, +9 bp insertion	CACTACCAGCAGCTC AAGAGGCAGAACTGG ^ CTGAGCCTC
	sM3- 9	II	-36 bp deletion, +8 bp insertion	GTCTTGAGGCTCAGA AGAAAGAGGCAGAAC ^ CGATCACT
	sM2- 11	II	-129 bp deletion	AACACATCCGGTACA AACTGATCACCACTC
	sM2- 12	IV	-3,459 bp and -405 bp deletion +403 bp and +28 bp insertion	ATGGCTTGATCGCTA AAATGAAGTGGTCTG GCCACTTTATTGGC TGGCCAGCAGAGGAA TCCGAAATGAAGTGG GAAAATGCTGAATTT
	sM3- 7	IV	approx. -5 kbp deletion, insertion	AGAATCCAGATGGAT ATCAATGTTGTGCAG
	sM2- 14	IV	approx. -5 kbp deletion, reverse-fragment insertion	AGCCCACAATGCCGC CATCGATCATTTGCA
	sM1- 9	IV	approx. -5 kbp deletion, inter-chromosomal translocation	TTTATTTCCACTTTT CAATATTACATAACA
	sM2- 6	IV	-7,432 bp deletion, +153 bp insertion and two reverse-fragments (+457 bp and +1,115 bp) insertion	CGCCAGCGACGCACG CGCTATTACGGGGTT GCGTCCAGTACGTGG GCGGGTTGTGGACCT CGCAGGCATTACGTG TGTAATTCTTCTATT

Fig. 3. Deletion mutations classified as classes I-A, I-B, II, and IV recovered from MMC-treated and untreated cells. A partial genetic map of the lambda EG10 transgene, including the *gam* and the *redBA* target regions of Spi$^-$ selection is shown. Horizontal bars represent regions deleted in Spi$^-$ mutants. Open bars represent the deleted regions of classes I-A, I-B, and II mutants, which have no rearrangements. Closed bars show class IV deletions, which have rearrangements within the deleted regions. An angled end of a bar denotes that the deletion positions have not been precisely determined. Junctions are indicated as a space between the left and right sequences. Microhomology sequences in the junctions are underlined. One of two microhomologies in the junctions that are underlined is deleted when the two DNA fragments are joined. (^) The insertion of a sequence in the deletion junction. All the mutants were analyzed with mutant codes. The first letter in the mutant code, 's' stands for Spi$^-$ mutants. 'M' stands for MMC-treated group and 'C' for the untreated control group. The third number is the ID number for the independent culture flask. The last number is the mutant ID number. The sM2-3 represents the Spi$^-$ mutants ID #3 in the MMC-treated flask #2.

Miscellaneous mutations including base substitutions in the *gam* gene were classified as class V (Table 1). In the MMC-treated group, tandem base substitutions at 5′-GG-3′ were observed.

3.3. Molecular characteristics of gpt mutations induced by MMC

To analyze MMC-induced point mutations, 45 mutations observed in the MMC-treated cells and 46 mutations derived from untreated control cells were identified at the sequence level (Table 2). Specific MFs of single base substitutions of G:C to T:A (substitutions of G to T or substitutions of C to A in Fig. 6) was 6.7-fold higher in the MMC-treated group than in the untreated group (26.3×10^{-6} versus 3.9×10^{-6}, Table 2). In the MMC-treated group, 19 of 26 (73%) single base substitutions was observed in the 5′-CG-3′ or 5′-GG-3′ sequence, in which MMC monoadducts were preferentially induced (Fig. 6) [23,24]. In the control group, 18 of 34 (53%) single base substitutions occurred at the 5′-CG-3′ or 5′-GG-3′ sequence (Fig. 6).

For insertion mutations with an insertion size larger than 2 bp, specific MF was 3.5×10^{-6} in the MMC-treated group, while no such mutations were observed in the control group (Table 2). The two mutations induced by MMC treatment were both 9 bp insertions (Fig. 6). One had a sequence change of 5′-GCGcagaagGCG-3′ to 5′-GCGcagaaggcgcagaagGCG-3′ in nucleotide 229–230 in the *gpt* gene, and the other had 5′-TCCcgccaatcTCC-3′ to 5′-TCCgccaatctccgccaatcTCC-3′ in nucleotide 438–439 (the sequences underlined

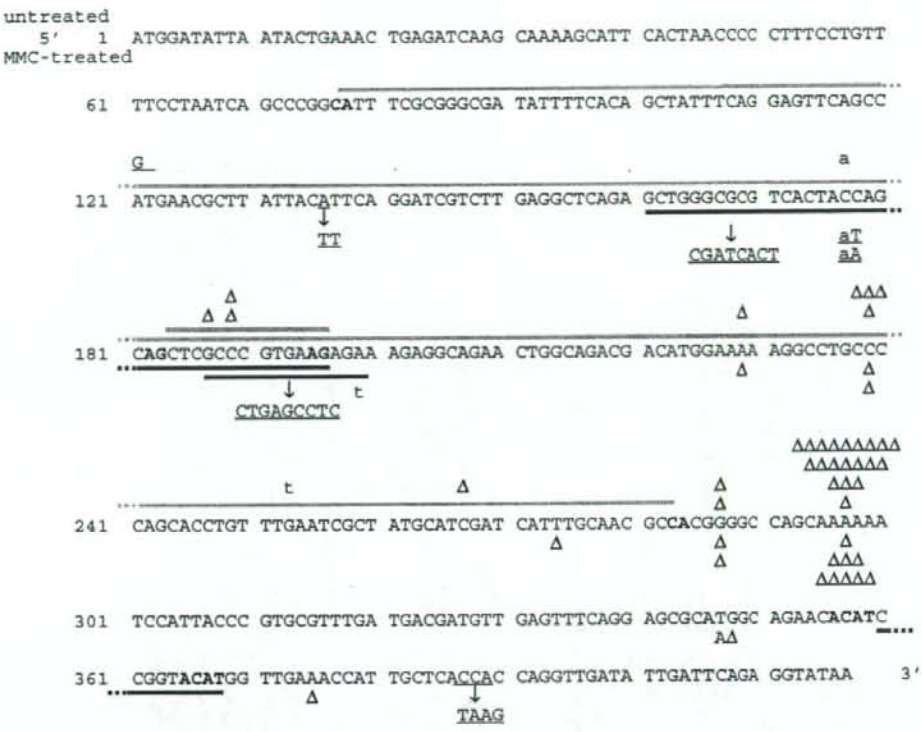

Fig. 4. Spi⁻ mutants of classes II, III-A, III-B, and V in the *gam* gene. The sequence from top to bottom represents the coding region of the *gam* gene. Mutations shown below the strands were detected in MMC-treated cells; those above the strands were observed in untreated cells. (Δ) Single base deletion. Sequence substitutions are underlined, the underlined sequences in the strands were substituted for the underlined sequence represented below the strands. Bars represent a deleted sequence in deletion mutations. The short homologous sequences associated with deletions are represented in bold. Two deletion mutations with sequence substitution in MMC-treated cells were substitutions of 5′-gctgggcgctcactaccagcagctcgcccgtgaag-3′ to 5′-cgatcact-3′ and 5′-gcccgtgaagaga-3′ to 5′-ctgagcctc-3′, and were classified as class II. The lowercase letters in the substituted sequences formed stop codon with adjoining two bases.

are altered sequences and the capital letters represent microhomology). In the former and latter mutants, 5′-cagaaggcg-3′ and 5′-cgccaatctc-3′, respectively, were repeated.

In deletion mutations larger than 2 bp, the specific MF in the MMC-treated group was 14 times higher than the untreated group (7.0×10^{-6} versus 0.5×10^{-6}, Table 2). In the MMC-treated group, four such deletions were identified (Fig. 6). They were an 8-bp deletion in 5′-CtcgcaagC-3′ of position 56–63, a 5-bp deletion in 5′-TaccgT-3′ of position 169–173, a 20-bp deletion in 5′-TCgcaaaaccggctggtcgTC-3′ of position 339–358, and a 329-bp deletion in 5′-CACTTcacatg· · ·aaagcgCACTT-3′ of position −3 to 326 in the *gpt* gene (not shown). All these deletions were enclosed by microhomology sequences. In the control group, one deletion with a size of 6 bp in 5′-GGCgaaGGC-3′ of position 241–246 was identified.

The specific MF of tandem base substitutions was 8.8×10^{-6} in the MMC-treated group, whereas no such mutations were observed in the untreated group. All five tandem base substitutions in the MMC-treated cells occurred in the 5′-GG-3′ or 5′-CG-3′ sequence, in which formation of MMC cross-links has been reported [15,16].

The specific MF of "others" was enhanced 14-fold by MMC treatments (7.0×10^{-6} versus 0.5×10^{-6}, Table 2). Four such MMC-induced mutations include a sequence substitution of 5′-TACCG-3′ to 5′-AACTA-3′ in position 122–126, a substitution 5′-CGG-3′ to 5′-AT-3′ in position 347–349, a −565-bp deletion accompanied by +1 bp insertion in position 11–575 (not shown) and a

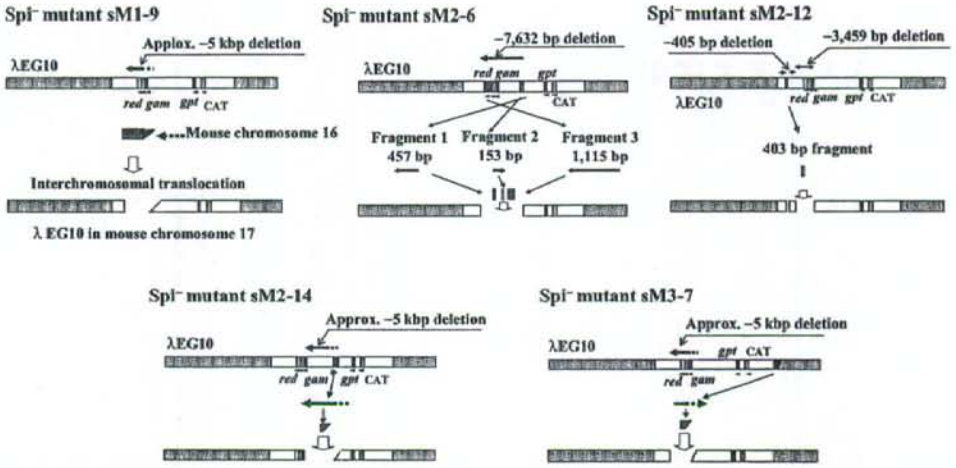

Fig. 5. Rearrangements induced in the Spi⁻ mutants derived from MMC-treated GDL1 cells. Complex deletions with insertions were observed in 5 Spi⁻ mutants. The upper bars in each mutant represent the lambda EG10 gene. The lower bars show mutants that have deletions and insertions resulting from MMC treatment. In the Spi⁻ mutant sM1-9, approximately 5 kbp were deleted. The inserted sequence was not found in the lambda EG10 gene but in chromosome 16 of the mouse genome. In Spi⁻ mutant sM2-6, 7632 bp including the *gam* gene sequence was deleted, and three DNA fragments within the deleted sequence, fragment 1 (457 bp), fragment 2 (153 bp), and fragment 3 (1115 bp), were inserted. The direction and order of the inserted fragments were different from that of the original sequence. In Spi⁻ mutant sM2-12, a fragment of 3459 bp including the *gam* gene was deleted and a fragment of 403 bp was inserted into the deletion site. In Spi⁻ mutant sM2-14, the deletion size was approximately 5 kbp. An inverted sequence existing approximately 6 kbp from the deletion site was inserted into the deletion junction. In Spi⁻ mutant sM3-7, the deletion size was approximately 5 kbp. A DNA fragment located approximately 18 kbp from the deletion site was inserted into the deletion site.

Table 2
Summary of *gpt* mutations derived from the GDL1 cells

Type of mutation	Control		MMC		*P* value[a]
	No. of mutants (%)	Specific MF[b] ($\times 10^{-6}$)	No. of mutants (%)	Specific MF[b] ($\times 10^{-6}$)	
Base substitution/single					
Transition					
G:C→A:T	13 (28.3)	6.4	7 (15.6)	12.3	0.18
A:T→G:C	3 (6.5)	1.5	2 (4.4)	3.5	0.31
Transversion					
G:C→T:A	8 (17.4)	3.9	15 (33.3)	26.3	<0.0001
G:C→C:G	1 (2.2)	0.5	1 (2.2)	1.8	0.40
A:T→T:A	4 (8.7)	2.0	0 (0.0)	0.0	0.58
A:T→C:G	5 (10.9)	2.5	1 (2.2)	1.8	1.00
Insertion					
+1A	2 (4.3)	1.0	0 (0.0)	0.0	1.00
+1T	3 (6.5)	1.5	2 (4.4)	3.5	0.31
>+2 bp	0 (0.0)	0.0	2 (4.4)	3.5	<0.05
Deletion					
−1A	1 (2.2)	0.5	0 (0.0)	0.0	1.00
−1G	2 (4.3)	1.0	0 (0.0)	0.0	1.00
−1C	2 (4.3)	1.0	2 (4.4)	3.5	0.22
>−2 bp	1 (2.2)	0.5	4 (8.9)	7.0	<0.05
Base substitution/tandem					
GG:CC→TC:AG	0 (0.0)	0.0	2 (4.4)	3.5	<0.05
GG:CC→TT:AA	0 (0.0)	0.0	2 (4.4)	3.5	<0.05
CG:GC→AA:TT	0 (0.0)	0.0	1 (2.2)	1.8	0.22
Others	1 (2.2)	0.5	4 (8.9)	7.0	<0.05
Total	46 (100)	22.7	45 (100)	78.9	<0.0001

[a] *P* values were determined using Fisher's exact test according to Carr and Gorelick [22].
[b] Specific MF was calculated by multiplying the total mutation frequency by the ratio of each type of mutation to the total mutation.

complex mutation, i.e., gM1-6 (Fig. 7). In this complex mutant, three DNA fragments were inserted into position 158–168 of the *gpt* gene, and the direction and the order of the inserted fragments were different from those of the original sequences. The original locations of fragment 1 (335 bp), fragment 2 (1092 bp), and fragment 3 (133 bp) were 17, 13, and 22 kbp, respectively, from the inserted position. A mutation in the control group of this class was a sequence substitution of 5′-CCG-3′ to 5′-ACC-3′ in position 278–280.

4. Discussion

Significant and dose-related increases in Spi$^-$ and *gpt* MFs of the GDL1 cells were observed after treatment with MMC (Fig. 2, Tables 1 and 2). In the in vivo experiment using *gpt* delta mice exposed to MMC [8], statistically significant increases of large deletion mutations (class I, Table 3) in Spi$^-$ mutants and tandem base substitutions at the 5′-GG-3′ or 5′-CG-3′ sequence (Table 4) in *gpt* mutants were seen. These mutations were also predominantly induced in GDL1 cells by MMC (Tables 3 and 4). In addition, MMC-induced complex mutations (class IV) in Spi$^-$ mutants and single base substitutions at G:C bp in the *gpt* mutants were observed in the GDL1 cells (Tables 3 and 4). Increase of these mutations was not observed in *gpt* delta mice treated with MMC [8]. Single base substitutions at G:C bp induced by MMC were also reported in another mammalian cell in vitro [25]. Monoadducts of MMC are probably responsible for single base mutations [26], and adducts are preferentially formed in the 5′-CG-3′ and 5′-GG-3′ sequences [23,24]. In fact, most of the single base substitutions were observed at guanines at the 5′-CG-3′ or 5′-GG-3′ sequences (Fig. 6). The GDL1 cell line was established from the genetic modification of introducing an artificially constructed expression unit for the SV40 T antigen gene into lung fibroblasts of *gpt* delta mice. The SV40 T antigen can immortalize fibroblasts through formation of complexes with p53 and interruption of p53-dependent growth suppression [27–29]. Hence, the normal function of p53 might be lost in the GDL1 cells.

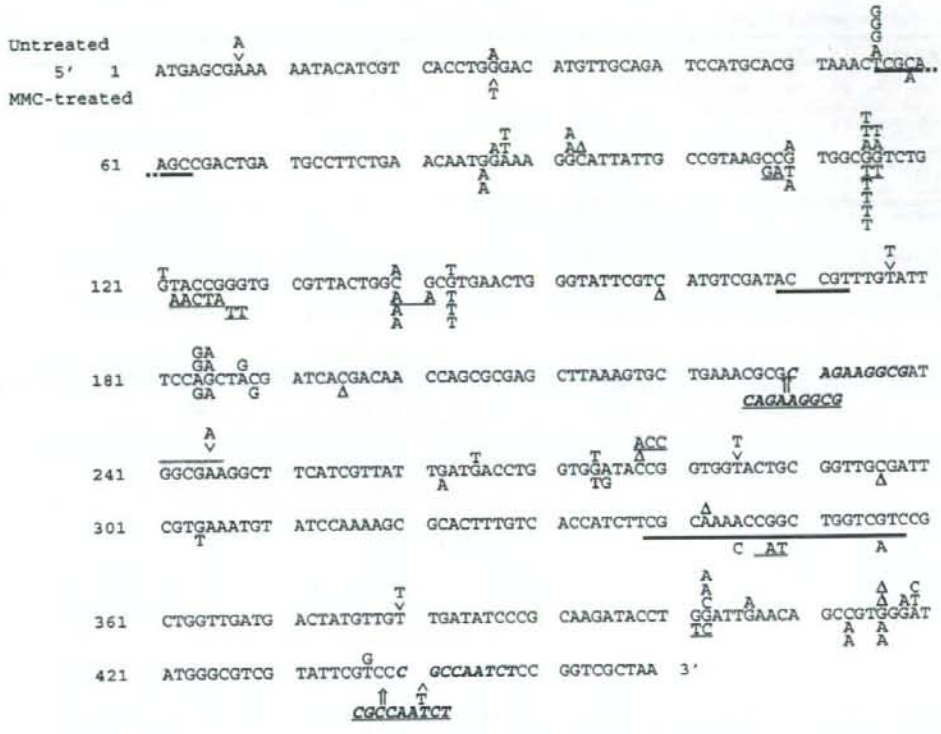

Fig. 6. Mutations in the *gpt* gene obtained from MMC-treated and untreated GDL1 cells. The sequence from top to the bottom represents the coding region of the *gpt* gene. Mutations shown above the sequence are from untreated cells and below from cells treated with MMC. (Δ and ∧) Single base deletions and one base insertion, respectively. Tandem base substitutions and sequence substitutions are underlined. Bars represent deleted sequences in deletion mutations. Inserted sequences are underlined and insertion positions are shown with arrows. The repeated sequences are shown in italicized boldface. In MMC-treated cells, a 329-bp deletion in nucleotide −3 to 326 (−3 indicates 3 bp prior to the first base of the first codon) and a 565-bp deletion accompanied by 1 bp insertion in position 11–575, and a complex rearrangement are not represented in Fig. 6 (see Fig. 7 for a complex rearrangement). One *gpt* mutant in untreated cells had two G:C to T:A mutations in nucleotide 121 and 143.

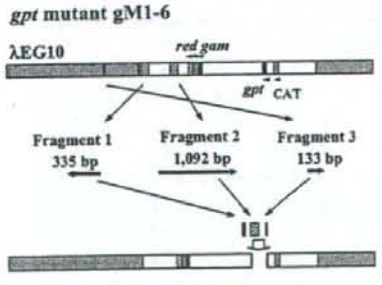

Fig. 7. Rearrangement induced in the *gpt* mutant derived from MMC-treated GDL1 cells. In *gpt* mutant gM1-6, three DNA fragments, fragment 1 (335 bp), fragment 2 (1092 bp), and fragment 3 (133 bp), were inserted into position of 158–168 of the *gpt* gene, and the directions and orders of the inserted fragments were different from that of the original sequence.

The p53 gene plays an important role in nucleotide excision repair (NER) [30–33] and NER activity decreased in cell lines transformed with the SV40 T antigen [34] and papillomavirus E6 genes [35]. Therefore, the potency of p53-dependent DNA repair pathways including NER might be different between GDL1 cells and *gpt* delta mice, which could account for the induction of single base substitutions and complex mutations (see below) in GDL1 cells.

Five complex mutations of Spi$^-$ (Fig. 5) and one rearranged mutant of *gpt* (Fig. 7) were observed in MMC-treated GDL1 cells. Comparison of the Spi$^-$ mutant in *p53*$^{+/+}$ and *p53*$^{-/-}$ *gpt* delta mice exposed to carbon-ion irradiation indicated that the induction of complex rearrangements was significantly accelerated by p53-knockout in the kidney, where p53 is highly expressed, but not in the liver, where p53 is weakly